Mechanical signals activate p38 MAPK pathway-dependent reinforcement of actin via mechanosensitive HspB1

Laura Hoffman[a,b], Christopher C. Jensen[a], Masaaki Yoshigi[a,c], and Mary Beckerle[a,b,d,*]
[a]Huntsman Cancer Institute, [b]Department of Biology, [c]Department of Pediatrics, and [d]Department of Oncological Sciences, University of Utah, Salt Lake City, UT 84112

ABSTRACT **Despite the importance of a cell's ability to sense and respond to mechanical force, the molecular mechanisms by which physical cues are converted to cell-instructive chemical information to influence cell behaviors remain to be elucidated. Exposure of cultured fibroblasts to uniaxial cyclic stretch results in an actin stress fiber reinforcement response that stabilizes the actin cytoskeleton. p38 MAPK signaling is activated in response to stretch, and inhibition of p38 MAPK abrogates stretch-induced cytoskeletal reorganization. Here we show that the small heat shock protein HspB1 (hsp25/27) is phosphorylated in stretch-stimulated mouse fibroblasts via a p38 MAPK-dependent mechanism. Phosphorylated HspB1 is recruited to the actin cytoskeleton, displaying prominent accumulation on actin "comet tails" that emanate from focal adhesions in stretch-stimulated cells. Site-directed mutagenesis to block HspB1 phosphorylation inhibits the protein's cytoskeletal recruitment in response to mechanical stimulation. HspB1-null cells, generated by CRISPR/Cas9 nuclease genome editing, display an abrogated stretch-stimulated actin reinforcement response and increased cell migration. HspB1 is recruited to sites of increased traction force in cells geometrically constrained on micropatterned substrates. Our findings elucidate a molecular pathway by which a mechanical signal is transduced via activation of p38 MAPK to influence actin remodeling and cell migration via a zyxin-independent process.**

Monitoring Editor
Valerie Marie Weaver
University of California, San Francisco

Received: Feb 2, 2017
Revised: Jul 24, 2017
Accepted: Jul 28, 2017

INTRODUCTION

Mechanical forces are sensed by cells and transduced into biochemical signals that drive changes in gene expression and influence cell fate (Discher *et al.*, 2009; Wozniak and Chen, 2009; Mammoto *et al.*, 2012). This ability to sense and respond to mechanical cues is essential during development and throughout an organism's life. Moreover, disturbance of mechanical homeostasis is associated with myriad disease phenotypes (Deanfield *et al.*, 2007; Chen, 2008; Fournier *et al.*, 2010; Ateshian and Humphrey, 2012). For a mechanical signal to influence biology, it must be converted to a chemical signal that is capable of regulating cell behavior and function; this is the process of mechanotransduction. A major challenge in cell biology is to ascertain the mechanistic details that underlie mechanotransduction.

A central element of a mechanotransduction pathway from the cell surface to the cell interior involves the coupling of cell-surface adhesion receptors, such as integrins, to mechanosensors that are themselves conformationally modulated in response to mechanical cues or adapted to recognize such force-induced changes (McGough *et al.*, 1997; Sawada *et al.*, 2006; del Rio *et al.*, 2009; Shimozawa and Ishiwata, 2009; Ehrlicher *et al.*, 2011; Hayakawa *et al.*, 2011; Uyeda *et al.*, 2011; Galkin *et al.*, 2012). Integrins are transmembrane heterodimers that bind extracellular matrix and anchor actin-rich stress fibers (SFs) at prominent membrane-substratum adhesion sites called focal adhesions (FAs) (Burridge *et al.*, 1988). Essential for maintaining tensional homeostasis, SFs are

This article was published online ahead of print in MBoC in Press (http://www.molbiolcell.org/cgi/doi/10.1091/mbc.E17-02-0087) on August 2, 2017.

*Address correspondence to: Mary C. Beckerle (Mary.beckerle@hci.utah.edu)

Abbreviations used: AI, alignment index; CMT2, Charcot-Marie-Tooth disease type2; DAPI, 4′,6-diamidino-2-phenylindole; FA, focal adhesion; F-actin, filamentous actin; G-actin, globular (monomeric) actin; GFP, green fluorescent protein; hsp, heat shock protein; MAPK, mitogen-activated protein kinase; MK2, mitogen-activated protein kinase–activated protein kinase 2; SF, stress fiber; SFTI, stress fiber thickness index; TAN line, transmembrane actin-associated nuclear line.

myosin-associated, contractile bundles of filamentous actin (F-actin). SFs are prominent in cultured cells, particularly fibroblasts, and also assemble in vivo when cells experience mechanical stress (Wong *et al.*, 1983; Byers *et al.*, 1984). FAs enable internal SF-generated contractile forces to be transmitted to the cell exterior and external mechanical signals to be communicated to the cell interior (Harris *et al.*, 1980; Wang *et al.*, 1993; Lauffenburger and Horwitz, 1996). As such, FAs are recognized as a major site for the transmission of physical cues from the cell exterior to interior (Geiger *et al.*, 2009; Yan *et al.*, 2015; Horton *et al.*, 2016).

The exposure of cells to mechanical stimulation results in remodeling of the actin cytoskeleton, providing an attractive system for the study of the mechanotransduction response. When fibroblasts are plated on a flexible substrate and subjected to uniaxial cyclic stretch, they reorient perpendicular to the stretch vector and undergo a SF thickening or "reinforcement" response (Yoshigi *et al.*, 2005; Hoffman *et al.*, 2012). The SF reinforcement response depends on the recruitment of LIM domain proteins, such as zyxin and paxillin, both of which contribute to the actin remodeling that occurs in response to mechanical stress (Yoshigi *et al.*, 2005; Smith *et al.*, 2010, 2013). Abrogation of the SF reinforcement response is evident in zyxin-null and paxillin-null cells, and this results in an increase in spontaneous SF breaks within the cells, illustrating that the mechanotransduction response that leads to SF remodeling and reinforcement is key to cytoskeletal homeostasis (Smith *et al.*, 2013; Smith *et al.*, 2014). Although several LIM proteins have now been implicated in the response of cells to mechanical force (Kim-Kaneyama *et al.*, 2005; Hirata *et al.*, 2008; Colombelli *et al.*, 2009; Schiller *et al.*, 2011), little is understood about the upstream signaling cascades that are activated as a prelude to the actin reinforcement response.

Mitogen-activated protein kinase (MAPK) signaling cascades are activated in mechanically stimulated fibroblasts (Nguyen *et al.*, 2000; Sawada *et al.*, 2001) as well as in organs such as the heart and lung when mechanical stress is elevated (Zhang *et al.*, 2000; Dolinay *et al.*, 2008). Activation of p38 MAPK signaling occurs in response to fluid shear stress (Li *et al.*, 1996), in response to pulling on magnetic beads attached to cells (Wang *et al.*, 2005), and in response to cyclic deformational strain (Chaudhuri and Smith, 2008). The p38 pathway is activated by multiple environmental stimuli that are transmitted via cell-surface proteins, including transmembrane growth factor receptors, receptor tyrosine kinases, and G-protein coupled receptors (Cuadrado and Nebreda, 2010; Hotamisligil and Davis, 2016; Rodriguez-Carballo *et al.*, 2016). Mechanical stimulation has been shown to activate the small G-protein Rap1 and MKK3/6 kinases that phosphorylate p38 (Sawada *et al.*, 2001). P38 MAPK signaling is also activated downstream of transmembrane integrin engagement via focal adhesion kinase and is antagonized by the protein tyrosine phosphatase PTEN (Aikawa *et al.*, 2002). Integrin engagement has also been shown to be required for the response of fibroblasts to uniaxial cyclic stretch (Yoshigi *et al.*, 2005), thus providing a link between FAs and mechanically sensitive MAPK signaling. Here we have interrogated the role of p38 MAPK signaling in the response of cells to uniaxial cyclic stretch and have uncovered a role for this pathway in the stretch-dependent actin-reinforcement response. We have explored the molecular mechanism by which stretch-activated p38 MAPK signaling influences the mechanotransduction response, defining the role of p38 MAPK-dependent phosphorylation of the small heat shock protein HspB1 (also known as mouse hsp25 and human hsp27) in the response of cells to mechanical stress.

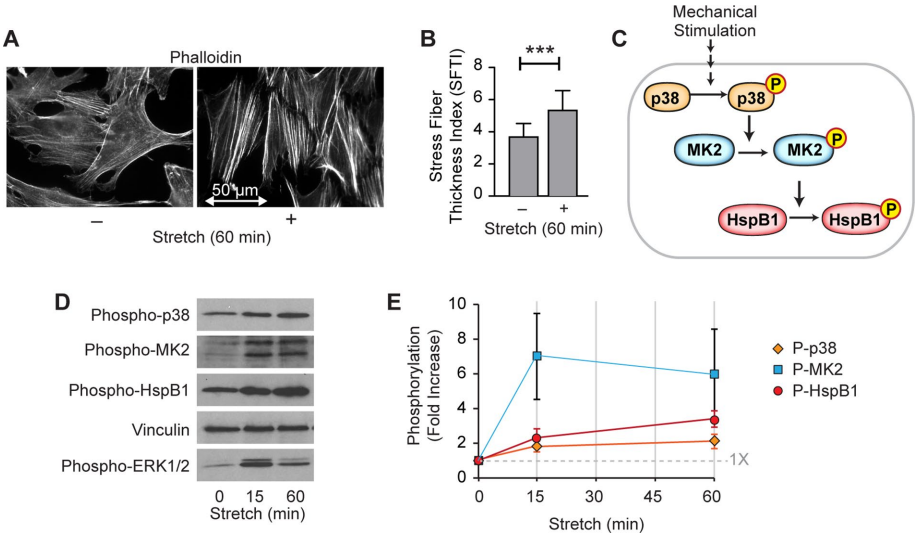

FIGURE 1: Uniaxial cyclic stretch promotes actin remodeling and activation of p38 MAPK signaling. (A) Mouse fibroblasts were stimulated by uniaxial cyclic stretch (15%, 0.5 Hz, 1 h) followed by detection of F-actin with fluorescently tagged phalloidin; the stretch direction is on the horizontal plane, indicated by a double-headed arrow scaled to 50 µm. (B) Comparison of the SFTI of unstretched and stretch-stimulated cells revealed a statistically significant increase in SFTI. Graph is mean with SD, ***$p < 0.0001$ was calculated using unpaired Student's *t* test that assumed Gaussian distribution and equal SD between populations, $n > 100$ SFTI measurements in >13 microscopic fields per group. (C) Schematic representation of p38 MAPK pathway. (D) Western immunoblot analysis (20 µg protein per lane) revealed the activation of the p38 MAPK pathway in response to uniaxial cyclic stretch, as illustrated by phosphorylation of p38, MK2, and HspB1. Immunoblot detection of vinculin confirms equal protein loading across lanes and detection of ERK1/2 activation confirms effective delivery of the stretch signal. (E) Quantitation of phosphorylation signals relative to unstretched samples (set at onefold baseline) illustrates the sustained activation of p38 signaling during the 60 min period of the stretch regimen, mean with SD as pooled from more than three independent stretch experiments.

RESULTS

Uniaxial cyclic stretch activates p38 MAPK and induces actin cytoskeletal remodeling

Despite the broad functional significance of a cell's ability to sense and respond appropriately to mechanical cues, the molecular mechanisms by which physical cues are converted to cell-instructive chemical information remain to be elucidated. The response of fibroblasts to mechanical stress can be studied by exposing the cells to a regimen of controlled uniaxial cyclic stretch. This type of stimulation induces alignment of fibroblasts perpendicular to the stretch vector and also promotes an actin remodeling response that results in actin SF reinforcement (Yoshigi *et al.*, 2005; Figure 1A). The actin SF reinforcement is evidenced by a thickening of the actin SFs that can be described quantitatively as the stress fiber thickness index (SFTI; Yoshigi *et al.*, 2005; Hoffman *et al.*, 2012; Figure 1B).

The molecular mechanism by which a mechanical signal influences cellular biochemistry is postulated to involve MAPK

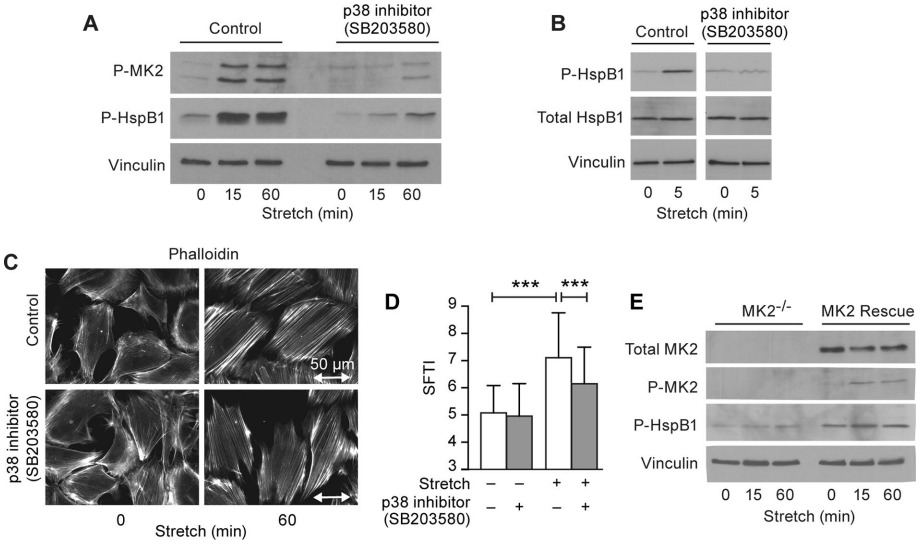

FIGURE 2: Inhibition of p38 MAPK signaling abrogates the stretch-induced actin SF reinforcement response. Mouse fibroblasts were preincubated with DMSO or p38 pathway inhibitor SB203580 (10 μM, 1 h) and were exposed to stretch stimulation (uniaxial cyclic stretch 15%, 0.5 Hz) followed by cell lysate preparation or fixation and staining. (A) Western immunoblot analysis of cell stretch response (15 min, 60 min) in the presence of p38 inhibitor SB203580. Control cells increase phospho-MK2 and phospho-HspB1 levels in response to stretch. Preincubation of cells with 10 μM SB203580 before and during stretch stimulation blocks the p38 activation of MK2 and HspB1. (B) Western immunoblot analysis to detect phosphorylated or total HspB1 in cell lysates (10 μg protein/lane) shows SB203580 inhibition of HspB1 phosphorylation within 5 min of stretch stimulation, while the total HspB1 levels are unaffected. Vinculin immunodetection confirms comparable protein loading. (C) Phalloidin-staining to visualize F-actin in unstretched and stretched cells under control or SB203580 treatment conditions. Double-headed arrow shows stretch direction and represents 50 μm scale. (D) SFTI analysis illustrates that inhibition of p38 MAPK abrogates the SF reinforcement response. Graph includes mean with SD (n = 161,160, 308, 372 roi, respectively). Statistical analysis was performed using an unpaired Student's t test assuming Gaussian distribution and equal SD between populations; ***p value < 0.0001. (E) Western immunoblot of stretch-stimulated cell lysates (15 μg protein/lane) from MK2$^{-/-}$ cells and MK2$^{-/-}$ cells expressing a rescue MK2 protein. Total MK2 and phospho-MK2 immunoblots show lack of MK2 in MK2$^{-/-}$ cells and restoration of MK2 and stretch-stimulated phospho-MK2 in the rescue cells. Phospho-HspB1 is significantly increased in the MK2 rescue cells. Vinculin shows equivalent protein loading.

signaling pathways and prior investigations have revealed the activation of ERK1/2 MAPK signaling in response to uniaxial cyclic stretch (Richard *et al.*, 2007; Boudreault and Tschumperlin, 2010; Cohen *et al.*, 2010; Hoffman *et al.*, 2012). Here we have explored whether p38 MAPK signaling is activated by uniaxial cyclic stretch of fibroblasts and could contribute to the actin remodeling response. As shown schematically in Figure 1C, p38 phosphorylates MAPK-activated protein kinase 2 (MK2; also referred to as MAPKAPK2), activating its kinase function and promoting the phosphorylation of a number of proteins, including HspB1, which has been previously implicated in the regulation of actin dynamics (Miron *et al.*, 1991; Benndorf *et al.*, 1994; Lavoie *et al.*, 1995; Huot *et al.*, 1997; Clarke and Mearow, 2013). On exposure to uniaxial cyclic stretch, mouse fibroblasts display elevated phosphorylation of p38, MK2, and HspB1 (Figure 1D), as visualized by Western immunoblot analysis using antibodies that specifically detect phospho-isoforms. Although consistent increases in phosphorylation occur in response to mechanical stimulation, it is noted that variable baseline phosphorylation of these proteins is observed in experimental replicates, which is likely attributable to stochastic stress signals experienced by the cultured cells. Immunoblot analysis using antibodies that detect total protein levels does not reveal any increase in levels of p38 pathway constituents (data not shown). Evaluation of the levels of the focal adhesion protein vinculin provides a protein loading control and monitoring of ERK1/2 activation confirms that the cells detected the mechanical stimulation (Figure 1D). Quantitative analysis of the kinetics of p38, MK2, and HspB1 phosphorylation in response to uniaxial cyclic stretch (Figure 1E) illustrates that mechanical stimulation activates the p38 signaling in a timeline that is consistent with a possible role in promotion of the actin SF reinforcement response.

Inhibition of the p38 pathway abrogates stretch-induced reinforcement of actin SFs

To test whether activation of the p38 pathway is required for the actin reinforcement response downstream of mechanical stress, we evaluated the actin stretch response in the presence of the p38 inhibitor SB203580 (Cuenda *et al.*, 1995; Guay *et al.*, 1997; Young *et al.*, 1997). Cells were preincubated with dimethyl sulfoxide (DMSO) (control) or with SB203580 for 1 h and then stimulated with uniaxial cyclic stretch in the presence of DMSO or SB203580. Phosphorylation of both MK2 and HspB1 occurs in DMSO-treated cells exposed to uniaxial cyclic stretch, whereas phosphorylation of both proteins is abrogated in cells exposed to the p38 inhibitor (Figure 2A). These findings are consistent with the hypothesis that the stretch-dependent phosphorylation of MK2 and HspB1 is largely attributable to activation of the p38 pathway. The p38 inhibitor-sensitive phosphorylation of HspB1 is observed within 5 min of stretch application under conditions where no corresponding increase in HspB1 protein is observed (Figure 2B). Although exposure to SB203580 does not result in dissolution of the actin cytoskeleton and drug-treated cells properly align SFs perpendicular to the stretch vector (Figure 2C), cells stretched in the presence of the p38 inhibitor display a statistically significant deficiency in the SF reinforcement response (Figure 2, C and D). To determine whether the kinase responsible for elevated phospho-HspB1 is MK2, we stretch-stimulated MK2-null and rescue cells (generously provided by Matthias Gaestel) (Ronkina *et al.*, 2007; Sousa *et al.*, 2007). The levels of phospho-HspB1 are increased in the MK2 rescue cells compared with MK2-null cells (Figure 2E), suggesting that MK2 is likely the kinase responsible for the phospho-HspB1 signal we are detecting. Although our findings clearly illustrate that elimination of MK2 abrogates the stretch-induced phosphorylation of HspB1, the MK2-null cells are transformed with SV40 large T antigen (Ronkina *et al.*, 2007) and thus cannot be directly compared with the other cell types used in this study. Moreover, we detect two MK2 isoforms in our WT fibroblasts consistent with previous reports while the rescue cell line expresses only one MK2 isoform (Ronkina *et al.*, 2007; Sousa *et al.*, 2007). Collectively our findings illustrate that p38 MAPK signaling contributes to the mechanotransduction response and caused us to focus our

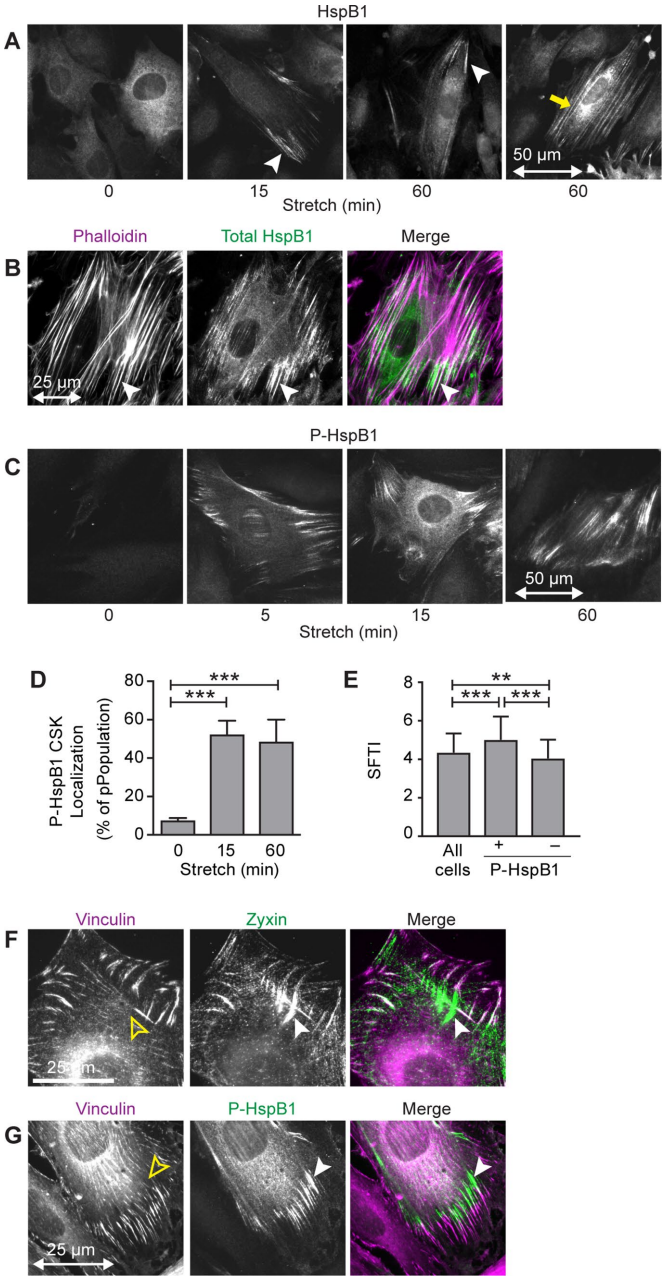

FIGURE 3: Phospho-HspB1 is recruited to discrete SF domains in response to uniaxial cyclic stretch. (A) Indirect immunofluorescence localization of total HspB1 in stretch-stimulated mouse fibroblasts shows diffuse cytoplasmic HspB1 distribution in unstretched cells and HspB1 recruitment to short linear elements within the cytoplasm of stretch-stimulated cells. Two examples of labeling are shown for the 60 min timepoint to illustrate that we observe HspB1 can be found at both SF termini (arrowheads) and full SFs (arrows) in stretched cells. (B) Double labelling of HspB1 and F-actin reveals that HspB1 displays a subcellular distribution that overlaps with actin SFs (arrowheads) but does not generally populate the entire expanse of transcellular SFs. (C) Indirect immunofluorescence localization of phosphorylated HspB1 shows a rapid accumulation of phospho-HspB1 in association with SF termini in stretched cells. Phospho-HspB1 is also detected on linear nuclear lines in some stretched cells. (D) Quantitation of the percentage of cells displaying discrete phospho-HspB1 localization under unstretched or stretched conditions compared across four independent experiments. (E) SFTI analysis of stretch-stimulated F-actin is presented as total population (4.3 SFTI, 251 roi) and then stratified for phospho-HspB1–positive cells (5.0 SFTI, 187 roi) and phospho-HspB1–negative cells (4.0 SFTI, 140 roi). Cells with phospho-HspB1 on the cytoskeleton generally have higher SFTI. (F) Double labeling of mouse fibroblast on coverslip with antibodies directed against vinculin (magenta) and zyxin (green). Scale bar is 25 μm. (G) Double labeling of stretch-stimulated fibroblast with antibodies directed against vinculin (magenta) and phospho-HspB1 (green). (F, G) The region of zyxin and phospho-HspB1 at comet tails (white arrowheads) that do not colocalize with vinculin (yellow arrowheads) is indicated. Double-headed arrows indicate the stretch vector and scale of 25 or 50 μm as designated. Graphs are shown as mean with SD. *P* values were determined by unpaired Student's *t* test assuming Gaussian distribution and equal SD between populations. $^{**}p < 0.001$, $^{***}p < 0.0001$, n.s. = not statistically significant.

attention on HspB1 as a potential candidate for contributing to stretch-induced actin SF remodeling.

HspB1, a downstream target of the p38 pathway, is recruited to the actin cytoskeleton in response to mechanical cues

HspB1 was previously identified as a regulator of actin filament assembly that copurifies with vinculin (Miron *et al.*, 1988, 1991). The p38-dependent phosphorylation of HspB1 in response to stretch raised the intriguing possibility that HspB1 might play a role in the actin remodeling that is induced by mechanical stimulation. If HspB1 contributes to the reinforcement of actin SFs downstream of mechanical stress, then we might expect to detect it in association with the actin cytoskeleton. As reported by others (Collier and Schlesinger, 1986; Lavoie *et al.*, 1995; Clarke and Mearow, 2013), we find that HspB1 displays a diffuse cytoplasmic distribution in unstretched (0 min of stretch) fibroblasts (Figure 3A). However, when cells are stimulated by exposure to uniaxial cyclic stretch for 15 or 60 min, HspB1 is frequently detected on linear elements within the cytoplasm that we postulated might correspond to subdomains of actin SFs (Figure 3A). The colocalization of HspB1 with actin SFs in stretched cells was confirmed by coincidence of the HspB1 immunofluorescence signal (arrowheads) with that of F-actin as detected by Phalloidin staining (Figure 3B). These findings illustrate that HspB1 is recruited to actin SFs in response to cell stretch.

Since HspB1 is phosphorylated in a p38-dependent manner in response to stretch, we investigated whether phospho-HspB1 is the isoform that is recruited to the actin cytoskeleton in response to mechanical stimulation. Immunostaining of unstretched or stretched cells with an antibody that recognizes phosphorylated HspB1 (Ser86) revealed that phospho-HspB1 becomes concentrated on linear cytoplasmic elements in response to uniaxial cyclic stretch (Figure 3C). The localization of phospho-HspB1 is prominent at the cell periphery and is also observed overlaying the nucleus in structures reminiscent of transmembrane actin-associated nuclear (TAN) lines (Luxton *et al.*, 2011) in some cells. Quantitative analysis of the percentage of cells that exhibited a discrete, SF-associated subcellular localization of phospho-HspB1 in response to stretch is shown in Figure 3D. Phospho-HspB1 is barely detectable in unstretched cells (<10% of cell population). In contrast, within 5 min (Figure 3C) we observe recruitment of phospho-HspB1 to subdomains of actin SFs in response to stretch that peaks with ~50% of cells displaying some cytoskeletal accumulation of phospho-HspB1 after exposure to a 60-min stretch regimen (Figure 3D). To evaluate whether there is a correlation between the detection of cytoskeletal-associated phospho-HspB1 and the reinforcement of actin SFs as evidenced by SFTI analysis, we compared the population-wide SFTI

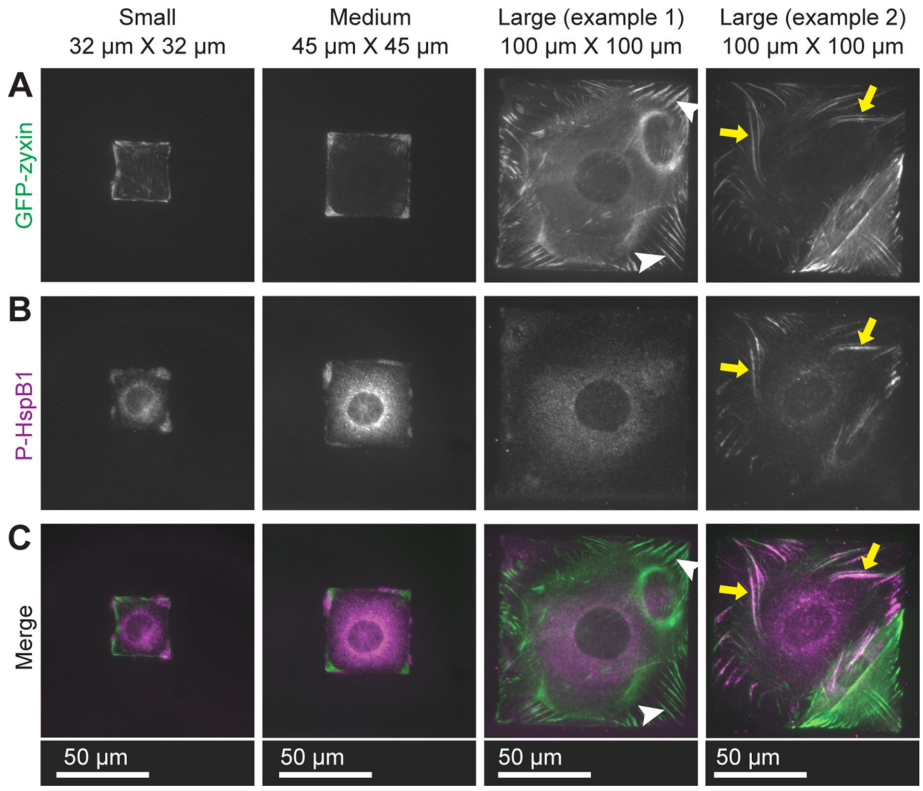

FIGURE 4: Localization of phospho-HspB1 on micropatterned substrates reveals accumulation at sites of ruffling and elevated traction force. GFP-zyxin expressing cells were plated on fibronectin islands of various dimensions (small [1024 µm^2], medium [2025 µm^2], large [10,000 µm^2]) and immunolabeled to detect phospho-HspB1. Both proteins are concentrated at the four corners of the square-shaped cells, with partially overlapping distributions. The large micropattern square induces the formation of prominent zyxin-rich comet tails (example 1) as was previously reported by Guo and Wang (2007). Phospho-HspB1 is colocalized with zyxin at some (large example 2, arrows) but not all (large example 1, arrowheads) of these structures. The scale bar of 50 µm is the same for all images.

measurement for stretched cells with the SFTI measurements from cells in the population that scored positive for cytoskeletal accumulation of phospho-HspB1 and those that scored negative for cytoskeletal accumulation of phospho-HspB1 after exposure to a 60-min stretch regimen. As shown in Figure 3E, we find that stretched cells that exhibit cytoskeletal accumulation of phospho-HspB1 also display a statistically significant enhancement of the SFTI response. The unstratified cell population exhibits an SFTI of 4.3 compared with 5.0 for cells with phospho-HspB1 cytoskeletal association and 4.1 for cells with no detectable cytoskeletal association of phospho-HspB1. Statistical analysis reveals that the cells segregate into two different populations based on their phospho-HspB1 cytoskeletal accumulation status, and that is strongly correlated with the SFTI measurements.

The terminal SF domains that associate with focal adhesions are often referred to as "comet tails" (Guo and Wang, 2007). The actin comet tails emanate from vinculin-rich FAs and are characterized by the presence of the LIM-protein zyxin (Figure 3F, arrowhead) (Beckerle, 1986; Crawford and Beckerle, 1991). Active actin polymerization and retrograde flow has been shown to occur at these discrete SF domains (Guo and Wang, 2007). In contrast with zyxin, which is detected both in focal adhesions and on comet tails (Figure 3F), phospho-HspB1 is enriched at actin comet tails of mechanically stimulated cells and displays only minimal overlapping distribution with vinculin as detected by indirect immunofluorescence (Figure 3G). Although the most striking and consistent distribution of phospho-HspB1 in stretched cells corresponds to actin comet tails, in the 50% of cells that display cytoskeletal association of HspB1, we observe diversity in the phospho-HspB1 staining patterns, having noted both variable staining intensity, as well as heterogeneity in extent of comet tail labeling and occasional labeling of transverse SFs (Supplemental Figure S1).

The elaboration of actin comet tails can be promoted by plating cells on square, micropatterned substrates (Parker *et al.*, 2002). Under these conditions, the accumulation of zyxin and the formation of zyxin-rich comet tails are concentrated at the four corners of the cells where ruffling and the strongest traction forces are observed (Wang *et al.*, 2002; Guo and Wang, 2007; Rape *et al.*, 2011). Therefore, to test whether the accumulation of phospho-HspB1 is enhanced at areas of strong traction forces, we plated green fluorescent protein (GFP)-zyxin expressing cells on micropatterned, fibronectin surfaces of various dimensions and examined the localization of both zyxin and phospho-HspB1 (Figure 4). Zyxin and phospho-HspB1 both accumulated at the corners of the square-shaped cells, indicating that the recruitment of both proteins is force sensitive. However, the two proteins did not display complete overlapping distributions. In the first image of a cell spread on the Large (10,000 µm^2) micropatterned area (example 1), zyxin comet tails are readily apparent at the corners (arrowheads) but phospho-HspB1 appears in a diffuse cytoplasmic distribution. In the second image showing cells plated on the large (10,000 µm^2) micropatterned area (example 2), one can observe overlapping distributions of zyxin and phospho-HspB1 at comet tails (Figure 4, arrows).

Robust recruitment of HspB1 to comet tails depends on sustained mechanical stimulation and is inhibited by cytochalasin D

To determine whether sustained mechanical stimulation is required for maintenance of HspB1 phosphorylation, cells were stretch stimulated for 1 h and then removed from stretch stimulation for another hour prior to fixation. Phospho-HspB1 increases on stretch stimulation and declines on removal of the stretch stimulation (Figure 5A). Immunolocalization studies show that phospho-HspB1's cytoskeletal accumulation declines on cessation of cell stretch (Figure 5B). The SFTI increases with stretch stimulation and also returns to baseline within 1 h after removal from stretch stimulation (Figure 5C), illustrating that SF reinforcement is a dynamic response that requires sustained mechanical stimulation. Treatment with cytochalasin D, a drug that binds to the barbed ends of actin filaments and prevents actin elongation (Flanagan and Lin, 1980; Brown and Spudich, 1981; Cooper, 1987; Peng *et al.*, 2011), under conditions that do not result in complete dissolution of SFs, abrogates the accumulation of phospho-HspB1 on SF termini (Figure 5D). These results are consistent with the view that the cytoskeletal localization of phospho-HspB1

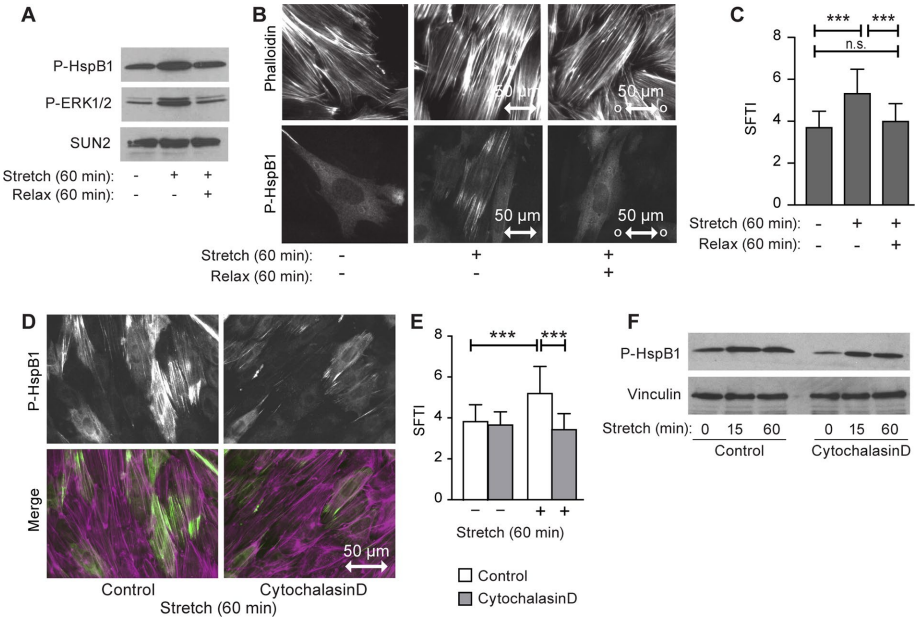

FIGURE 5: Stretch-dependent phosphorylation and recruitment of HspB1 to the actin cytoskeleton. Cells were subjected to a "yoga" regimen of uniaxial cyclic stretch (15%, 0.5 Hz, 60 min) followed by relaxation (60 min). (A) Western immunoblot analysis (25 µg protein per lane) reveals that activation of HspB1 by phosphorylation is promoted by uniaxial cyclic stretch and that maintenance of stretch signaling is required to sustain HspB1 phosphorylation. Stretch control phospho-ERK1/2 signal is similarly stretch stimulated and then decreased by removal of stimuli. Loading control is nuclear envelope protein SUN2. (B) Comparison of unstretched, stretched, and stretched/relaxed cells reveals the stretch-induced accumulation of phospho-HspB1 on actin SFs (phalloidin), with diminished accumulation on cell relaxation. (C) SFTI analysis reveals that SF reinforcement increases with stretch stimulation and then declines to baseline levels when the stretch signal is removed (n = 259, 355, 289 roi, respectively). (D) Exposure to cytochalasin D (250 nM, preincubation 1 h, 7 µg protein) during stretch stimulation (15% uniaxial, 0.5 Hz, 15 min and 60 min) compromises the recruitment of phospho-HspB1 (green) to actin SFs (phalloidin, magenta) and abrogates the SF reinforcement response (E, SFTI analysis; $n = 259$, 149, 283, 147 roi, respectively). (F) Western immunoblot shows stretch-induced phosphorylation of HspB1 continues in the presence of cytochalasin D. Vinculin immunodetection confirms equal protein loading. Graphs are presented as mean with SD, p values were derived from unpaired t tests that assumed Gaussian distribution and equal SDs between populations, $^{***}p < 0.0001$, n.s. = not statistically significant.

depends on the availability of free F-actin barbed ends. The stretch-induced SF reinforcement response is also compromised in response to treatment with cytochalasin D (Figure 5E), whereas the stretch-induced phosphorylation of HspB1 persists (Figure 5F), illustrating that it is the recruitment of HspB1, not its activation by phosphorylation, that is perturbed in cytochalasin D–treated cells.

Phosphorylation of HspB1 is required for its mechanically sensitive cytoskeletal accumulation

Since the stretch-induced recruitment of HspB1 to cytoskeletal structures occurs concomitant with increased phosphorylation of HspB1, we tested the possibility that stretch-induced phosphorylation directs the cytoskeletal recruitment of HspB1. Murine HspB1 is phosphorylated by MK2 on two serine residues in response to p38 MAPK activation (Stokoe *et al.*, 1992) (Figure 6A). We generated site-specific mutations in a GFP-tagged variant of HspB1 to enable direct visualization of the phospho variants in unstretched and stretched cells. The HspB1-GFP proteins were expressed in wild-type (WT) fibroblasts using a lentiviral delivery system and subsequent fluorescence-activated cell sorting (FACS) to isolate a population enriched in GFP-expressing cells. Importantly, C-terminally tagged HspB1 faithfully recapitulates the subcellular distribution of endogenous phospho-HspB1 in stretched cells (Figure 6B). Western immunoblot analysis shows the expression of wild-type HspB1-GFP as well as two mutant variants: the unphosphorylatable S2A variant in which Ser15 and Ser86 are mutated to alanine and the S2E variant in which Ser15 and Ser86 are mutated to the phosphomimetic residue glutamic acid (Figure 6C). WT, S2A, and S2E-HspB1-GFP do not display cytoskeletal localization in unstretched cells (Figure 6, D–F). Thus the phosphomimetic variant S2E is not sufficient to drive actin SF accumulation in the absence of a bona fide mechanical signal. Compared to WT HspB1 (Figure 6D), the S2A variant fails to associate with the actin cytoskeleton in response to stretch stimulation (Figure 6E), consistent with the view that phosphorylation of HspB1 on Ser15 and/or Ser86 is necessary for cytoskeletal recruitment. The phosphomimetic S2E variant displays visible recruitment to the actin cytoskeleton in response to stretch (Figure 6F). This recruitment typically appeared less robust compared with WT protein, possibly reflecting preferential cytoskeletal association of the endogenous HspB1 that is present in the GFP-expressing cells.

HspB1-null cells generated by CRISPR/Cas9 genome editing are deficient in stress fiber remodeling

A CRISPR/Cas9 nuclease strategy was employed to disrupt the murine *HSPB1* gene to define the phenotypic consequences of loss of HspB1 function in cells (Figure 7A). Two regions in exon 1 were targeted (target sequences 23 and 27), and multiple cell lines were isolated and screened for HspB1 status. Immunoblot analysis of the parental WT cells and two independently derived CRISPR lines (lanes A and B) illustrate that HspB1 protein is not detected in the CRISPR lines, whereas upstream control proteins p38 and MK2 remain at WT levels (Figure 7B). The HspB1-null cells are readily propagated in cell culture and adhere to plastic dishes and glass coverslips. However, HspB1-null cells display abrogated spreading compared with WT cells on coverslips coated with increasing concentrations of the extracellular matrix fibronectin, as assessed by cell area measurements 3 h after plating the cells (Figure 7C). Cell morphology and FA status were assessed by staining cells plated for 3 h on coverslips coated with 10 µg/ml fibronectin (Figure 7D). Vinculin-rich FAs are detected in the HspB1-null cells; however, the FAs often appear smaller and less robust than in wild-type controls under these short-term culture conditions. Comparison of the actin cytoskeletons of unstretched parental WT cells to the HspB1-null cells does not reveal a consistent alteration in F-actin content by visual inspection (Figure 7E) or by SFTI analysis (Figure 7F), suggesting that HspB1 is not essential for baseline maintenance of the actin cytoskeleton in cultured fibroblasts. In response to uniaxial cyclic stretch, HspB1-null cells align perpendicular to the stretch vector comparable to wild-type cells; however, the actin reinforcement response is abrogated in HspB1-null cells compared with wild-type cells (Figure 7F).

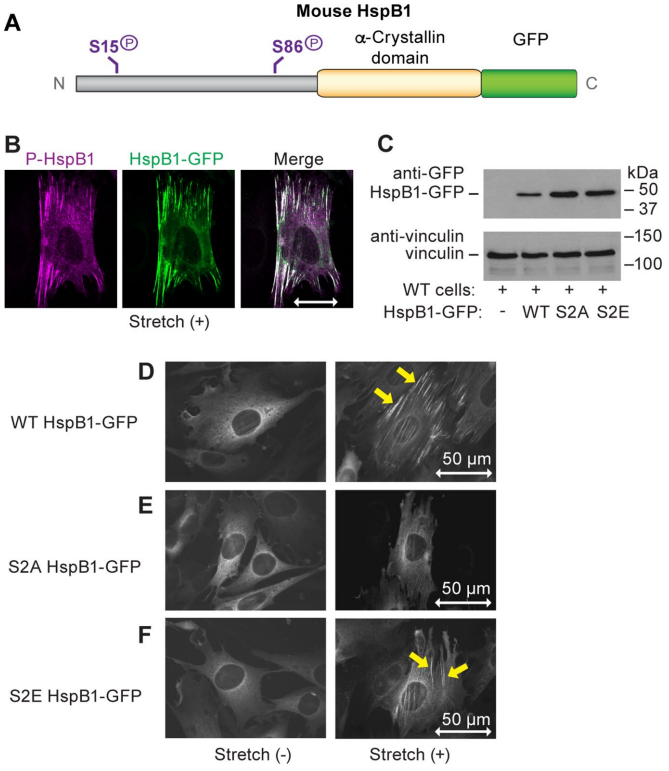

FIGURE 6: Site-directed mutagenesis reveals the role of phosphorylation of HspB1 for its cytoskeletal recruitment. (A) Schematic representation of GFP-tagged murine HspB1 protein illustrating primary p38 MAPK pathway MK2-dependent phosphorylation sites at Serine15 and Serine86 and the alpha-crystallin domain. (B) Demonstration that C-terminally tagged HspB1-GFP (green) faithfully recapitulates the subcellular distribution of endogenous phospho-HspB1 (magenta) following stimulation of cells with uniaxial cyclic stretch. In the Merge image, the overlapping distribution of green and magenta is white. (C) Site-directed mutagenesis was deployed to convert serines 15 and 86 to either alanine (S2A) or glutamic acid (S2E). Western immunoblot analysis (20 μg cell lysate/lane) with antibody directed against GFP reveals expression of GFP-tagged WT or mutant variants of HspB1 in WT cells with vinculin detection as a loading control. Antibodies specific for GFP detect a single protein band with mobility at the expected range for the fusion protein, comigrating with the 50-kDa molecular weight marker. (D–F) Immunofluorescence microscopy of unstretched or stretched (15%, 0.5Hz, 1 h) cells harboring the (D) GFP-tagged WT HspB1 or the phosphorylation site variants, (E) S2A, or (F) S2E exhibit typical HspB1 recruitment to cytoskeleton (yellow arrows) for WT and S2E proteins. Mutation of serines 15 and 86 to alanine abrogates the recruitment of HspB1 to the actin cytoskeleton in response to uniaxial cyclic stretch. Double-headed arrow of 50 μm scale indicates stretch direction in the horizontal plane.

HspB1-null cells display enhanced cell migration

The establishment of zyxin-rich actin comet tails is promoted by mechanical cues and is inversely correlated with cell migration (Guo and Wang, 2007). Zyxin-null cells display increased migration relative to their wild-type counterparts, consistent with the view that zyxin acts as a negative regulator of cell migration (Hoffman *et al.*, 2006). Given the localization of phospho-HspB1 on focal adhesion-associated actin comet tails, we postulated that elimination of HspB1 expression might affect cell migration. We used time-lapse microscopy to compare the migratory behaviors of the parental WT cells and the 2 HspB1-null cell lines. Cells were seeded to confluence into small chambers that were removed prior to microscopy, giving an even starting line to follow cell migration. In this directional migration assay, the HspB1-null cells consistently migrated farther than the parental WT cells in the same amount of time (Figure 8, A and B). During the 12-h observation period, WT cells migrated an average distance of 239 μm, whereas HspB1-null cells A and B migrated an average distance of 332 and 360 μm, respectively, demonstrating a 45% increase in net migration when HspB1 protein was eliminated. The average velocity for each cell type was determined by analysis of multiple independent experiments (Figure 8C). WT cells migrated consistently slower than either HspB1-null cell, suggesting that HspB1 acts as a regulatory brake during the process of cell migration. To demonstrate that the enhanced migratory behavior of HspB1-null cells was specifically due to the loss of HspB1, we compared the HspB1-null cells with rescue cells programmed to reexpress HspB1. To reconstitute HspB1 expression in the CRISPR/Cas9 edited HspB1-null cells, we generated a CRISPR/Cas9 nuclease-resistant HspB1 construct by mutating the protospacer adjacent motif (PAM). The HspB1-null cells engineered to reexpress HspB1 displayed HspB1 expression comparable to the parental WT cells (Figure 8D). Cell migration approached WT levels by reintroduction of HspB1 (Figure 8E). These data illustrate that HspB1 acts as a negative regulator of cell migration.

HspB1 and Zyxin contribute independently to the actin SF remodeling response to uniaxial cyclic stretch

Since both zyxin (Yoshigi *et al.*, 2005; Hoffman *et al.*, 2012) and HspB1 associate with the actin cytoskeleton in response to mechanical cues and both contribute to the SF reinforcement response downstream of uniaxial cyclic stretch, we explored whether these two proteins act in the same or parallel pathways. Unlike zyxin, HspB1 is not associated with actin SFs in unstimulated cells (Supplemental Figure S2), but both proteins accumulate on actin SFs in response to mechanical cues. Elimination of HspB1 expression fails to perturb either zyxin expression levels (Figure 9A) or zyxin recruitment to actin SFs in response to uniaxial cyclic stretch (Figure 9B). We observed that the accumulation of zyxin on SFs of stretched HspB1-null cells appears diminished relative to what occurs in WT cells and postulate that this is due to the abrogated actin remodeling response in cells lacking HspB1 (Figure 7, E and F). Reciprocally, elimination of zyxin does not have deleterious effects on the HspB1 response to stretch. The phosphorylation of HspB1 in response to stretch is evident in zyxin-null cells (Figure 9A) and HspB1's accumulation on actin comet tails in stretched cells occurs independent of zyxin (Figure 9C). These results suggest that the HspB1 and zyxin responses to stretch occur by independent, mechanically sensitive pathways. If this were the case, then we would expect the SF remodeling and reinforcement response to be more seriously compromised in double-mutant cells than in either of the single-mutant cells. To explore this possibility, we used the CRISPR/Cas9 genome strategy presented in Figure 7 to mutagenize the *HSPB1* gene in our previously described zyxin-null cells (Yoshigi *et al.*, 2005; Hoffman *et al.*, 2006). As can be seen in Figure 9D, we have generated cells that lack detectable zyxin or HspB1 protein by Western immunoblot analysis. The double-mutant cells display vinculin-rich FAs and F-actin SFs when plated on glass coverslips (Figure 9E); although we noticed some subtle qualitative differences in the cytoskeletal organization of the double mutant cells, these were difficult to quantitate in unchallenged cell populations. When HspB1/zyxin double-null cells are challenged by exposure to uniaxial cyclic stretch, we observe alignment of actin SFs perpendicular to the stretch vector both by visual inspection of phalloidin-labeled cells (Figure 9F) and

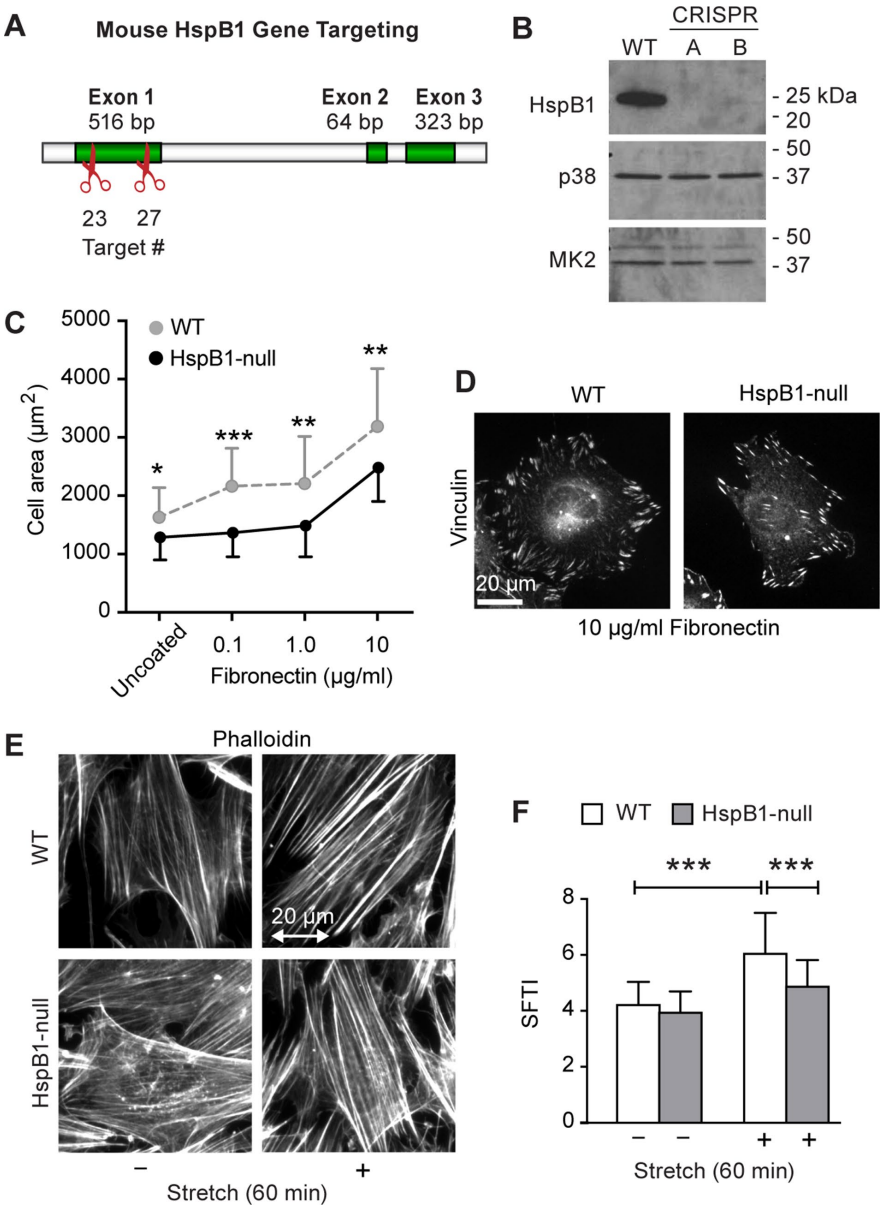

FIGURE 7: Generation of HspB1-null cells by CRISPR/Cas9 genome editing. (A) Schematic representation showing the genome editing scheme. The *HspB1* gene has three exons; the two CRISPR/Cas9 nuclear targeting sites in Exon 1 are marked as target 23 and target 27. (B) Western immunoblot (10 μg protein per lane) with the parental WT cells shows loss of HspB1 expression in the two independently edited and isolated cell lines A and B. Elimination of HspB1 expression does not affect p38 or MK2 levels within cells. (C) Quantification of cell area for adhesion and spreading (3 h in media with 10% serum) on coverslips that were either uncoated or coated with 0.1 μg/ml, 1 μg/ml, or 10 μg/ml fibronectin to promote integrin engagement and focal adhesion formation (mean with SD; n>26 cells measured per condition). The HspB1-null cells lag behind the WT cells in spreading on fibronectin. (D) Vinculin immunolocalization in WT cells and HspB1-null cells on fibronectin-coated coverslips. (E) Use of fluorescent phalloidin to stain F-actin in WT or HspB1-null cells reveals that elimination of HspB1 expression does not result in actin deficits that are consistently evident by visual inspection. Actin filaments are present in both unstretched and stretched HspB1-null cells and SF alignment downstream of application of uniaxial cyclic stretch persists in the absence of HspB1 while the actin reinforcement is impaired. The stretch vector is represented by double-headed arrow of 20 μm scale. (F) Graph of SFTI analysis for Phalloidin-stained WT and HspB1-null cells in unstretched and stretched conditions (mean with SD; $n > 300$ roi per condition). Although not completely inhibited, elimination of HspB1 results in a statistically significant reduction in the SF reinforcement response to stretch stimulation, illustrating that HspB1 contributes in an appreciable way to the response of cells to mechanical stimulation. Graphs plotted as mean with SD; p values (*$p < 0.05$, **$p < 0.001$, ***$p < 0.0001$) were derived from unpaired t tests assuming Gaussian distribution and equal SDs between populations.

by quantitative analysis of the SF Alignment Index (Figure 9G). In contrast, the HspB1/zyxin double-null cells display a striking deficit in the SF remodeling and reinforcement response downstream of uniaxial cyclic stretch as quantified by SFTI (Figure 9H). This actin reinforcement deficit was greater than that observed in either the HspB1-null or zyxin-null cells (Figure 9H). In addition to the lack of SF reinforcement in HspB1/zyxin double-null cells, we observe the presence of readily visible phalloidin-labeled aggregates (Figure 9, F and I; open arrowheads). These phalloidin-stained structures are not labeled by DAPI, indicating that they do not colocalize with cell nuclei and thus likely represent cell fragments or intracellular aggregates of filamentous actin. These findings illustrate that the capacity of cells to respond to mechanical stress depends on parallel, complementary pathways involving HspB1 and zyxin. Moreover, the elimination of both proteins results in a synthetic deterioration of the integrity of the actin cytoskeleton in cells exposed to cyclic stretch.

DISCUSSION

Mechanical forces are generated and transmitted by cells and these forces are critical for the regulation of cell shape, motility, and growth control (Discher *et al.*, 2009; Wozniak and Chen, 2009; Mammoto *et al.*, 2012; Iskratsch *et al.*, 2014). The role of mechanical force in shaping biological behavior is now a focal point for research in cell biology, developmental biology, biophysics, and bioengineering. Here we have shown that exposure of mouse fibroblasts to uniaxial cyclic stretch induces phosphorylation of p38 MAPK, activating a canonical kinase cascade (Stokoe *et al.*, 1992; Landry and Huot, 1995; Guay *et al.*, 1997; Kayyali *et al.*, 2002). This results in MK2-dependent phosphorylation of the small heat shock protein, HspB1, its localization to discrete SF subdomains, the reinforcement of actin SFs, and reduced cell migration (Figure 10). Our findings that elimination of HspB1 function in the context of mechanical stimuli has consequences to actin remodeling and cell motility provide new insight into the regulated role of HspB1 in cells.

The *HSPB1* gene is a ubiquitously expressed member of an ancient, highly conserved family of molecular chaperones that bind unfolded proteins under conditions of proteotoxic stress, preventing function-disrupting protein aggregation (Ellis and Hemmingsen, 1989; Rothman, 1989; Jakob *et al.*, 1993; Mymrikov *et al.*, 2011). Our findings raise the intriguing possibility that mechanical stress results in a conformational

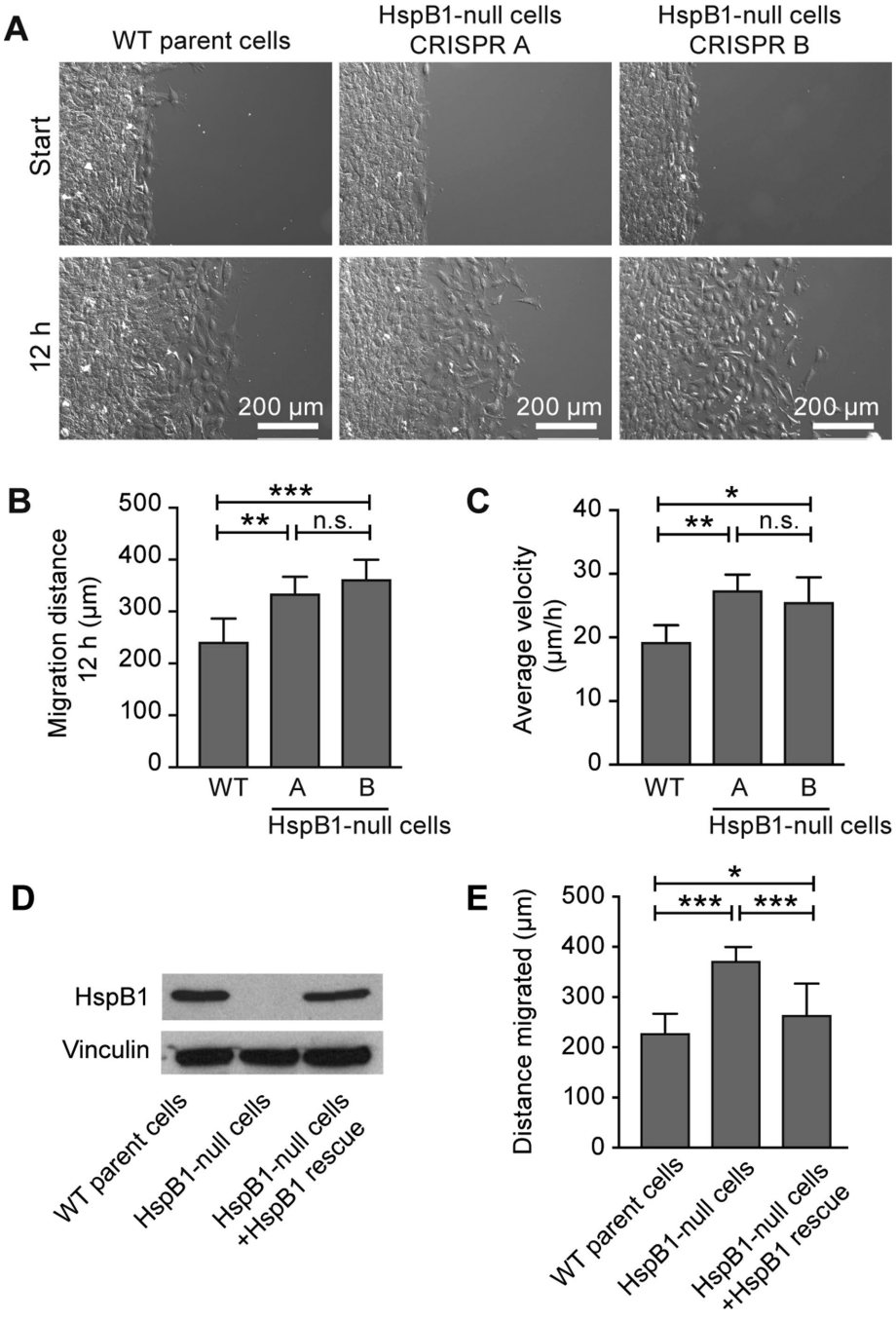

FIGURE 8: HspB1-null cells display enhanced cell migration. (A) Time-lapse microscopy was used to evaluate cell migration and compare the migratory behavior of cells from the parental WT line, as well as two independently derived HspB1-null lines, CRISPR A and CRISPR B. Cells were cultured to confluence within a confined area (Ibidi chambers) and then the barrier was removed, enabling directed cell migration from a well-defined edge. Migration of cells outward from the confluent cell island was monitored for 12 h. Fields of cells are shown at the beginning and at 12 h completion. Example time-lapse movies for WT, HspB1-null A, HspB1-null B cells are included as Supplemental Data. (B) Graph of 12 h migration distances for each cell type are shown from a single time-lapse experiment (9 measurements for each cell type) and the migration difference was reproduced in at least three independent experiments. WT cells migrated an average of 239 µm, HspB1-null A cells migrated an average of 332 µm, and HspB1-null B cells migrated an average of 360 µm over the 12 h period. (C) Graph of average velocity for each cell type showed a persistent migration difference in HspB1-null cells (four independent migration experiments). (D) Western immmunoblots (10 µg protein per lane) of WT parental cells, HspB1-null cells, and rescue HspB1 cells show the rescue HspB1 expression level approaches WT expression levels. Vinculin loading control confirms unchanged expression regardless of HspB1 status. (E) Quantitation of directed cell migration from a defined edge (Ibidi chambers) over a 12 h period. WT parental cells migrated an average of 230 µm (18 measurements), HspB1-null cells migrated an average of 372 µm (18 measurements), and HspB1 rescue cells migrated an average of 265 µm (18 measurements), suggesting that reexpression of HspB1 returned the cells to almost WT migration. Graphs are mean with SD; p values (*$p < 0.05$, **$p < 0.001$, ***$p < 0.0001$, n.s. = not significant) were determined using an unpaired t test that assumed Gaussian distribution and equal SDs between populations.

change in actin that is detected by HspB1. In addition to its generally accepted role as a protein chaperone, HspB1 was identified as a contaminant that copurifies with vinculin and acts as a potent inhibitor of actin polymerization (Miron *et al.*, 1988, 1991). Subsequent biochemical studies of purified HspB1 revealed that unphosphorylated HspB1 forms large oligomers, binds stoichiometrically to monomeric actin (G-actin), and inhibits actin polymerization in vitro (Benndorf *et al.*, 1994; Mounier and Arrigo, 2002; Salinthone *et al.*, 2008). Thus HspB1 is reported to act as an actin monomer sequestering protein that prevents precocious actin polymerization.

Several studies have suggested that HspB1's function as an actin regulator is influenced by posttranslational modification. Phosphorylation of HspB1 by MK2 in vitro induces dissociation of oligomeric complexes and release of HspB1-bound actin monomer to promote actin assembly (Huot *et al.*, 1997; An *et al.*, 2004; During *et al.*, 2007; Damarla *et al.*, 2009). Models that incorporate these established biochemical properties of HspB1 suggest an attractive mechanism for how mechanical signals might be converted into a biochemical output that could modulate the actin response in a phosphorylation-dependent manner (Gerthoffer and Gunst, 2001; Mounier and Arrigo, 2002; Salinthone *et al.*, 2008). However, historical efforts to localize HspB1 in cells has revealed only a diffuse cytoplasmic distribution (Collier and Schlesinger, 1986; Lavoie *et al.*, 1995; Clarke and Mearow, 2013), a finding that called into question the physiological relevance of HspB1's ability to interact with actin in vitro. We reasoned that if HspB1 were involved in the actin remodeling response downstream of mechanical stress, a cytoskeletal localization might be evident only in cells exposed to a mechanical stimulus. Indeed, we show here that HspB1 is associated with discrete regions of the

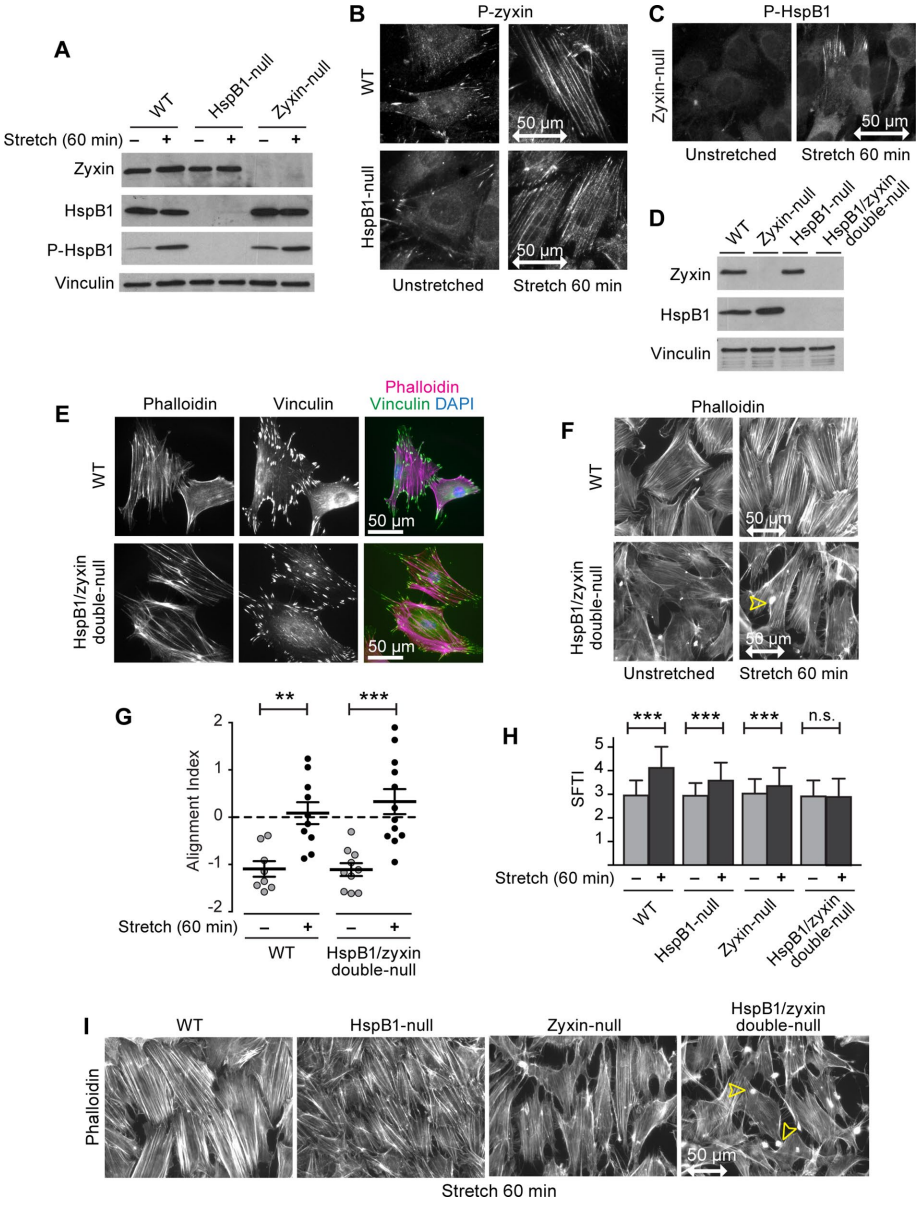

FIGURE 9: Parallel pathways of HspB1 and zyxin in the stretch-stimulated actin response. (A) Western immunoblot of cells lysates (10 μg/lane) of unstretched and stretched pairs (0, 60 min) from WT cells, HspB1-null cells, and zyxin-null cells. Zyxin (B72) signal is equivalent in the WT and HspB1-null cells but is absent from the zyxin-null cells, while the HspB1 signal is absent from the HspB1-null cells. Stretch-stimulated increase in phospho-HspB1 is maintained in the zyxin-null cells. Vinculin loading control confirms equal protein amounts in each lane. (B) Immunofluorescence staining of zyxin stretch response in WT cells shows zyxin focal adhesion distribution moves to stretch-stimulated actin. In HspB1-null cells, zyxin accumulation along stretch-stimulated actin SFs persists. (C) Immunofluorescence detection of phospho-HspB1 is low in unstretched zyxin-null cells and increases and localizes to the cytoskeleton in stretch-stimulated zyxin-null cells, as we previously described in WT cells (Figure 3). (D) Western immunoblot of WT, zyxin-null, HspB1-null, and HspB1/zyxin double-null cell lysates (10 μg protein/lane). Zyxin is detected in WT and HspB1-null cells. HspB1 is detected in WT and zyxin-null cells. Both zyxin and HspB1 are undetectable in the HspB1/zyxin double-null cells. Vinculin loading control shows comparable protein loading for all four cell types. (E) Immunofluorescence localization of F-actin (phalloidin, magenta) and vinculin (green) in WT cells and in HspB1/zyxin double-null cells. In unstimulated cells, the actin cytoskeleton and focal adhesions are maintained in HspB1/zyxin double-null cells. Scale bar is 50 μm. (F) Phalloidin staining of unstretched and stretch-stimulated WT cells reveals actin remodeling, reinforcement, and realignment perpendicular to stretch vector. In contrast, the HspB1/zyxin double-null cells fail to reinforce their actin filaments, and aggregates of actin (arrowhead) are detected. (G) Alignment analysis using distribution kurtosis on phalloidin-stained images indicated alignment perpendicular to the horizontal stretch vector increased with stretch stimulation of both cell types, and it was not different between WT and HspB1/zyxin double-null cells. The alignment index is graphed as mean with SEM, and *p* values were determined by unpaired *t* tests assuming Gaussian distributions with equal SD between populations. (H) SFTI analysis of unstretched (gray bars) and stretch-stimulated (black bars) cells (WT, HspB1-null, zyxin-null, HspB1/zyxin double-null). Unstretched/Stretched SFTI: WT cells 3.0/4.2, HspB1-null cells 3.0/3.6, zyxin-null 3.1/3.4, HspB1/zyxin double-null cells 3.0/3.0. Only HspB1/zyxin double-null cells were not significantly different (n.s.) by SFTI analysis. SFTI is graphed as mean with SD, greater than 100 measurements per condition, and unpaired *t* tests assumed Gaussian distributions with equal SD between populations. (I) Stretch-stimulated cells (uniaxial cyclic stretch, 15%, 0.5 Hz, 60 min) stained for F-actin (phalloidin) display alignment perpendicular to the stretch vector and variable stress fiber thickening (see H) depending on the presence or absence of HspB1, zyxin, or both proteins. Aggregates of F-actin in the HspB1/zyxin double-null cells are indicated by arrowheads. The stretch vector is represented by double-headed arrow of 50 μm scale. $^{**}p < 0.001$, $^{***}p < 0.0001$, n.s. = not significantly different.

actin cytoskeleton in cells subjected to uniaxial cyclic stretch (Figure 3, A–C). Moreover, we have uncovered a relationship between our ability to detect HspB1 in association with the actin cytoskeleton and the cell's SFTI, providing a correlation between cytoskeletal accumulation of HspB1 and SF remodeling and reinforcement (Figure 3E). Future analysis of what attracts HspB1 differentially to actin comet tails and dissection of the detailed molecular mechanism by which HspB1 contributes to actin SF remodeling and reinforcement will further enhance our understanding of the response of cells to mechanical stress.

Given the correlation between HspB1 cytoskeletal accumulation and SF reinforcement, it is of interest to understand what physiological conditions influence the association of HspB1 with the actin cytoskeleton. Our studies have revealed that retention of HspB1 in association with the actin cytoskeleton depends on sustained delivery of mechanical cues (Figure 5, A–C). Consistent with our findings that HspB1's association with the actin cytoskeleton is promoted by mechanical stimulation, HspB1 was identified as a contractility-dependent component of FAs in unbiased proteomic studies (Kuo *et al.*, 2011; Schiller *et al.*, 2011). Although the application of uniaxial cyclic stretch induces a pronounced enhancement

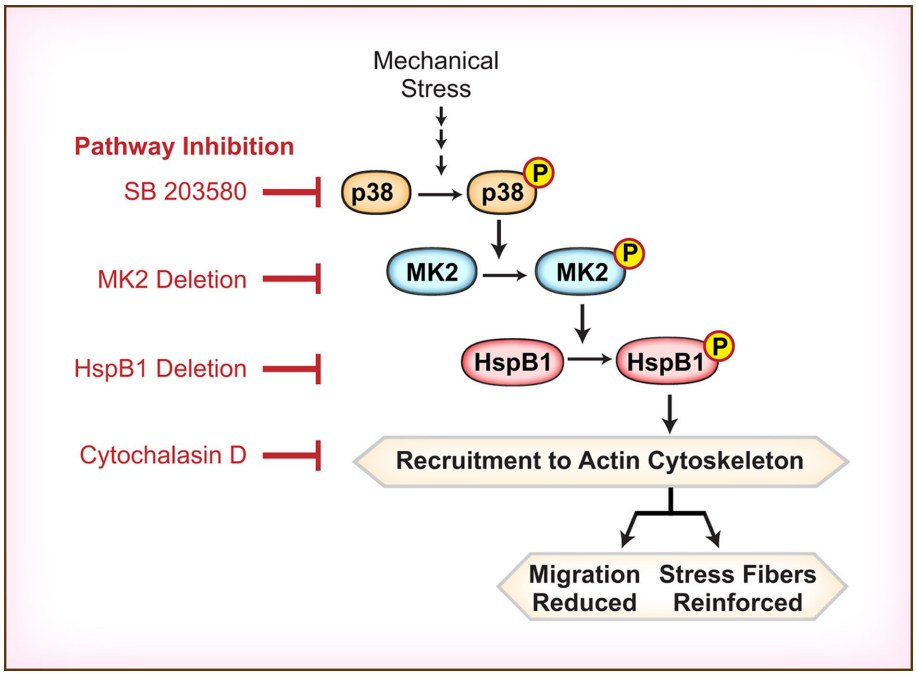

FIGURE 10: Model illustrating a proposed mechanism by which p38 MAPK signaling influences the response of cells to mechanical stress. Stretch activation of p38 results in phosphorylation and recruitment of HspB1 to the actin cytoskeleton, especially actin comet tails. Elimination of HspB1 function abrogates SF reinforcement and promotes cell migration. The HspB1 pathway provides a previously uncharacterized mechanism for mechanotransduction that is independent of the role of zyxin in stretch-induced actin remodeling.

of HspB1 association with cytoskeletal elements, it is important to note that SF association of HspB1 is not uniformly observed on all SFs within a cell nor is cytoskeletal association observed in all cells. The underlying reason for the heterogeneous accumulation of HspB1 on SF subdomains of individual cells is not understood. It is possible that some threshold level of mechanical stress is required for recruitment of HspB1 to the cytoskeleton and that depends on cell orientation relative to the stretch vector or other factors; it is possible that cytoskeletal accumulation of HspB1 is short lived and the protein is thus not captured uniformly in large cell populations visualized at a single arbitrary timepoint, or it is possible that HspB1 association with the cytoskeleton is regulated by secondary physiological cues that vary from cell to cell and remain to be elucidated. Analysis of the subcellular localization of fluorescently labeled HspB1 in living cells subjected to controlled mechanical stimulation will help to distinguish among these and other possibilities.

It is notable that phospho-HspB1 accumulates predominantly at FA-proximal actin comet tails that emanate from vinculin-rich FAs. These SF domains represent sites of elevated tension and actin assembly that are promoted by mechanical signals such as those engendered by substrate stiffness, geometrical constraints, or stretching forces (Wang *et al.*, 2002; Guo and Wang, 2007; Rape *et al.*, 2011). We previously reported that zyxin is present both in FAs and in actin comet tails (Beckerle, 1986; Crawford and Beckerle, 1991). Others have found that zyxin-rich comet tails are induced when cells are plated on stiff substrates and geometrically constrained micropatterned substrates, and they represent sites of dynamic retrograde actin and zyxin flux that is correlated with actin assembly (Guo and Wang, 2007). Our discovery of phospho-HspB1 at actin comet tails along with zyxin supports the notion that both proteins contribute to the mechanical stress response. Confirmation of that hypothesis was provided by the demonstration that mutant cells lacking both HspB1 and zyxin fail to launch an actin SF reinforcement response when exposed to uniaxial cyclic stretch (Figure 9H). In addition, when the double-mutant cells are challenged by exposure to mechanical stress, they accumulate aggregates of phalloidin-stained material (Figure 9, F and I). These unusual actin structures may result when strained SFs break and retract in a myosin-dependent manner (Smith *et al.*, 2010; Chapin *et al.*, 2012) or could occur via some other mechanism that remains to be identified.

An important contribution of our work is the demonstration that the phosphorylation of HspB1 is necessary but not sufficient to promote association with the actin cytoskeleton in living cells. Use of site-directed mutagenesis to create a mutant variant of HspB1 that lacks the two best characterized MK2-dependent phosphorylation sites (S2A-HspB1) enabled us to demonstrate that phosphorylation of HspB1 is critical for its stretch-stimulated recruitment to the actin cytoskeleton (Figure 6, D–F). Generation of an HspB1 variant (S2E-HspB1) designed to mimic a constitutively phosphorylated HspB1 in cells revealed that the presence of a constitutively "active" HspB1 is not sufficient to promote cytoskeletal association, as evidenced by the fact that no actin localization of S2E-HspB1 is observed in unstretched cells (Figure 6F). The ability of the S2E-HspB1 variant to accumulate in association with actin SFs exclusively in stretched cells (Figure 6F) illustrates the fidelity of the protein construct and that accumulation of HspB1 on the actin cytoskeleton requires both the posttranslational modification of HspB1, as well as the creation of cytoskeletal docking sites in response to mechanical stimulation. The accumulation of HspB1 at actin comet tails, which are established sites of actin polymerization and retrograde flow, raised the possibility that HspB1 was attracted to free-barbed ends of actin filaments, which are concentrated at these regions (Symons and Mitchison, 1991; Gupton *et al.*, 2007). Our demonstration that low-dose cytochalasin D inhibits the accumulation of phospho-HspB1 at actin comet tails is consistent with the view that free F-actin barbed ends are required for the targeted recruitment of HspB1 to SFs (Figure 5D). Thus we postulate that the application of mechanical force promotes both the availability of free barbed ends and the posttranslational modification of HspB1, enabling cytoskeletal recruitment of HspB1 and SF reinforcement.

Disturbance of HspB1 function causes distal hereditary motor neuropathy and Charcot-Marie-Tooth disease type 2 (CMT2), the most common inherited neuromuscular disease in humans (Evgrafov *et al.*, 2004; Houlden *et al.*, 2008). CMT2 is a disorder characterized by axonal peripheral neuropathy (Evgrafov *et al.*, 2004). Five autosomal dominant mutations in human HspB1 that cause CMT2 or distal hereditary motor neuropathy have been identified (Evgrafov *et al.*, 2004; Houlden *et al.*, 2008), and each of these residues is conserved in murine HspB1. The mechanism by which HspB1 mutations contribute to peripheral neuropathy is not understood. Given the critical role of the actin cytoskeleton for axon guidance, growth cone dynamics, and neuronal function (Dent and Gertler, 2003), it is intriguing to consider the possibility that these disorders

result from impairment of the neuronal cytoskeletal response to mechanical stress.

Collectively our findings highlight the role of p38 MAPK signaling in the mechanotransduction response and elucidate the role of a ubiquitous small heat shock protein in cytoskeletal remodeling and reinforcement in the face of mechanical challenge. We have provided a new framework for understanding the response of cells to mechanical cues by implicating a p38 MAPK signaling cascade and the downstream target, HspB1, as part of the mechanotransduction response (Figure 10). We show that phosphorylated HspB1 is recruited to actin comet tails that are established sites of mechanical tension and actin polymerization. Perturbation of the p38-MK2-HspB1 pathway with chemical inhibitors or genetic loss of function mutants results in a decreased actin SF remodeling and reinforcement response and increased cell migration. Prior studies have illustrated that HspB1 expression increases dramatically in cells exposed to high temperature and the protein accumulates on actin SFs in heat-challenged cells (Miron *et al.*, 1991; Bryantsev *et al.*, 2002), consistent with the idea that accumulation of HspB1 on the cytoskeleton is protective. Enhanced cell motility of HspB1-null fibroblasts is consistent with the inverse relationship of cell migration to comet tail formation (Guo and Wang, 2007) and with a report that HspB1-null mice display increased neutrophil migration in a wound closure model (Crowe *et al.*, 2013). The novel, p38-regulated roles of HspB1 in the response to mechanical stress raise questions about how p38 is activated by mechanical cues and whether other effectors downstream of p38 play central roles in mechanotransduction. Further analysis of these questions is warranted given both the physiological significance of the mechanotransduction response and current knowledge of the complexity of the p38 MAPK signaling network.

MATERIALS AND METHODS

Reagents

Antibodies for vinculin (Sigma V-9131), phospho-p38 and total p38 (Cell Signaling Technology #4511 & #9212), phospho-MK2 and total MK2 (Cell Signaling Technology #3007 & #3042), phospho-HspB1 (Cell Signaling Technology #9709 for human hsp27 phosphorylated on Ser82 and for mouseSer86) and total hsp25 (Cell Signaling Technology #2442 and Enzo Life Sciences ADI-SPA-801), phospho-ERK1/2 (Cell Signaling Technology #4370), phospho-JNK (Cell Signaling #4668), SUN2 (Abcam #124916), GFP (Living Colors #632381), phospho-zyxin (Cell Signaling Technology #8467), and zyxin (Beckerle Lab B71 and B72) were used as previously described (Hoffman *et al.*, 2003, 2006); zyxinB72 antibody is now commercially available (EMD Millipore ABC1387). AlexaFluor conjugated secondary antibodies and Phalloidin, along with 4′,6-diamidino-2-phenylindole (DAPI) were used as recommended (Molecular Probes/Invitrogen). Horseradish peroxidase–conjugated secondary antibodies (GE Healthcare) were used for Western immunoblots. P38 inhibitor SB203580 (Cell Signaling Technology #5633) and actin inhibitor cytochalasin D (Sigma #c8273) were resuspended in DMSO and used as directed by manufacturer.

Cells

Wild-type (WT) mouse fibroblast and GFP-zyxin cells were isolated and cultured as described previously (Hoffman *et al.*, 2006) in high-glucose DMEM complete (DMEMc) supplemented with pyruvate, glutamine, penicillin/streptomycin (Invitrogen), and 10% fetal bovine serum (Hyclone Labs, Logan, UT). MK2-null and rescue cells were provided by Matthias Gaestel and cultured as described (Ronkina *et al.*, 2007; Sousa *et al.*, 2007).

Mutagenesis

To generate the HspB1 S2A phospho-mutant, Ser15 AGC was mutated to Ala *GCT* and Ser86 AGC was mutated to Ala *GCT*, using a Quik Change site-directed mutagenesis kit (Agilent Technologies). To generate the HspB1 S2E phospho-mutant, Ser15 AGC was mutated to Glu *GAA* and Ser86 AGC was mutated to Glu *GAA*. The S2A and S2E mutants were generated in a pDONR221 Gateway recombination plasmid (Invitrogen). After DNA sequencing to confirm mutations, the clones were subsequently Gateway cloned into a pLenti6.3/V5 plasmid with a GFP tag (Invitrogen) for transfection into 293FT cells. Packaged virus from the 293FT cells was used to transduce wild-type mouse fibroblasts previously described (Hoffman *et al.*, 2006). The virally transduced cells were selected for resistance in 2.5 μg/ml blasticidin (Invitrogen).

CRISPR/Cas9 genome editing

HspB1-targeting sequences for CRISPR/Cas9 genome editing (Ran *et al.*, 2013) were designed and constructed by Timothy Dahlem, (University of Utah Mutation Generation and Detection Core; http://cores.utah.edu). To generate HspB1-null cells, Cas9 HspB1 fusion plasmids that encoded 5′ CGTGCCCTTCTCGCTGCTGC 3′ [CRISPR plasmid 23] and 5′ GGTCTCGGAGATCCGACAGA 3′ [CRISPR plasmid 27], both in exon 1 of the *HSPB1* gene, were transfected into 293 FT cells to generate CRISPR plasmid-containing lentivirus. The parental WT mouse fibroblasts previously described (Hoffman *et al.*, 2006) were virally transduced, and cells were selected for resistance in 2.5 μg/ml Puromycin (Invitrogen). Two independently targeted and isolated cell lines (CRISPR 23 "A" and CRISPR 23/27 "B") were used in experiments presented here. The *HSPB1* gene in CRISPR 23 A cells was sequenced and found to have a 253-base-pair deletion following the ATG start, which would result in a frame shift and multiple stop codons. HspB1 protein status was assessed by Western immunoblot analysis and by immunofluorescence localization using HspB1-specific antibodies and both CRISPR 23 A cells and CRISPR 23/27 B cells were determined to be null for HspB1 protein.

To generate an untagged HspB1 construct that was CRISPR/Cas9 nuclease resistant and could be reintroduced into HspB1-null cells as a "rescue" construct, the PAM site sequence 5′ to the start of the guide sequence in the *HspB1* gene was conservatively mutated from CGG (Arg) to ACG (Arg), creating a caspase 9–resistant expression construct. This rescue construct was virally transduced into the HspB1-null cells using the same viral production and expression protocol used to generate the original HspB1-null CRISPR 23 A cells (described above).

To generate the HspB1/zyxin double-null cells, the HspB1-targeting CRISPR plasmid 23 was used as described above on fibroblasts originally isolated from zyxin-null mice (Hoffman *et al.*, 2006). HspB1 protein status was assessed by Western immunoblot analysis to confirm the cells were null for both HspB1 and zyxin.

Uniaxial cyclic stretch, stress fiber thickening, and alignment analysis

Cells were stretch stimulated using a custom-designed system previously described (Yoshigi *et al.*, 2005). Briefly, cells were seeded onto precoated (25 μg/ml collagen I and 2 μg/ml fibronectin) silicone membranes (2.2 million cells onto three 26 × 33 mm membranes in a 10-cm plate) and grown to confluence overnight. Cells were either subjected to uniaxial cyclic stretch (15%, 0.5 Hz, up to 1 h) and then lysed and proteins harvested for immunoblot analysis or fixed (3.7% formaldehyde 15 min) for cell staining and microscopy (Yoshigi *et al.*, 2005; Hoffman *et al.*, 2012). For stretch experiments with

inhibitors (SB203580 at 10 μM; cytochalasin D at 250 nM), cells on membranes were preincubated for 1 h prior to stretch, and the stretch was performed in media with fresh inhibitor added. SFTI analysis of phalloidin-stained cells utilized a custom erosion/brightness decay software written in LabView (National Instruments) and previously described (Yoshigi *et al.*, 2005). Multiple stress fibers in multiple cells in >10 microscopic fields were measured (regions of interest, roi) for relative SFTI within single experiments in at least three independent stretch experiments. Stress fiber alignment analysis was performed as previously described (Yoshigi *et al.*, 2003; Yoshigi *et al.*, 2005). (For source code, contact M. Yoshigi.) Briefly, local stress fiber orientation was calculated by Sobel filter algorithm, and orientation histograms were obtained from ~400 cells. Distribution kurtosis of orientation histogram was designated as the alignment index. Higher alignment values indicate more aligned stress fibers (perpendicular to stretch vector), zero being mesokurtic (Gaussian distribution).

Immunofluorescence microscopy

Cells seeded onto glass coverslips or onto stretch-silicone membranes were fixed (15 min in 3.7% formaldehyde/phosphate-buffered saline) and then permeabilized (5 min in 0.5% Triton X-100), blocked (1 h in 5% normal goat serum), and incubated with antibodies as recommended by suppliers. Cell images were captured with a Zeiss Axiophot fluorescence microscope (Zeiss 40X NeoFluor 0.75 NA dry objective and Zeiss 63X ApoChromat 1.4 NA oil objective), Zeiss AxioCamMRm camera, Zeiss AxioVision version 4.8.1 software. Quantitation of phospho-HspB1 (Cell Signaling Technology Antibody #9709) localization patterns utilized images from at least 10 microscopic fields (>50 cells total for each stretch condition). Image sets were collected with identical camera settings throughout each experiment, and images were evaluated for cytoskeletal distribution on screen. The phospho-HspB1 localization signals were quantitated for four independent stretch and stain experiments.

For the fibronectin dose–response experiment, 30,000–60,000 WT cells and HspB1-null cells were seeded into a 12-well dish with glass coverslips that were uncoated or precoated with 0.1 μg/ml, 1 μg/ml, or 10 μg/ml fibronectin. The cells were incubated in DMEMc+10% serum for 3 h and then fixed and stained as described above. The spreading experiment was performed three times with similar results. For cell area quantitation, cells were outlined and measured (National Institutes of Health [NIH] FIJI ImageJ, v.2.0.0), with graph presentations and analysis using Graph Pad Prism software.

Western immunoblot analysis

Protein concentration of cell lysates were measured (Pierce Coomassie Protein Assay) and proteins (7.5–30 μg/lane, described in the figure legends) were electrophoresed through denaturing 15% polyacrylamide gels (Bio-Rad) and transferred onto nitrocellulose filters. Antibodies were diluted as recommended by the manufacturers and detected by HRP-conjugated antibodies and enhanced chemiluminescence (GE Healthcare). Quantitation of Western immunoblots to compare x-fold increase utilized the Analyze/Gels module of FIJI (NIH ImageJ) with the signals in unstretched lanes considered as onefold. Western immunoblot results were confirmed in at least three independent experiments.

Micropatterned substrates

A custom panel (20 mm × 20 mm) of square micropatterned adhesive areas (20 μg/ml Fibronectin) of increasing sizes of small 1024 μm^2 (32 × 32 μm), medium 2025 μm^2 (45 × 45 μm), and large 10,000 μm^2 (100 × 100 μm) (Cytoo chip, Grenoble France) were placed in a six-well plate. Cells were seeded (60,000 cells/well) and allowed 4 h to adhere and spread. Formaldehyde was added directly to the media to 3.7% concentration and cells were fixed for 15 min, followed by permeabilization, staining, and microscopy as described under *Immunofluorescence microscopy*.

Migration

Glass-bottom 12-well cell culture plates (Invitro Scientific PR-1.5HN) containing two-well culture insert chambers (Ibidi #80209) were seeded at 23,000 cells per insert chamber and grown for 24 h to confluent density. To begin the cell migration assay, the insert chambers were removed and cells were given fresh DMEMc + 10% fetal bovine serum media, and cells migrated out from the edge in a directed manner. Using a Nikon Ti Eclipse microscope and 10× objective with DIC, Nikon Elements software, and Pathology Devices environmental chamber (37°C, 5% CO_2, 70% humidity), multiple microscopic fields were imaged for 12–18 h at 10-min intervals. Image analysis and migration distances were measured with FIJI (NIH ImageJ). For each cell type, three microscopic fields were measured across the top, middle, and bottom of the field for a total of nine measurements per cell type. For the migration rescue experiments, six microscopic fields were measured as above for a total of 18 measurements per cell type. Cell migrations were compared between multiple cell types run within the same experiment, and migration experiments were performed at least three independent times.

Statistical analysis

Graphs are presented as mean with SD, and *p* values are noted in the figure legends with $p < 0.05$ considered statistically significant. The horizontal lines above the graphs identifies the two groups compared using unpaired Student's *t* tests that assumed a Gaussian distribution and equal SDs between populations and were calculated using Prism 6 software (Graph Pad). *$p < 0.05$, **p value < 0.001, ***p value less than 0.0001, comparisons that were not statistically significant (n.s.) are designated or not shown.

Figure preparation

Cell images were processed with Photoshop CC and assembled as figures in Illustrator CC (Adobe). Graphs were constructed in Prism 6 (GraphPad, San Diego CA).

ACKNOWLEDGMENTS

We are grateful to Timothy Dahlem at the University of Utah Mutation Generation and Detection Core Facility and Mike Redd at the University of Utah Fluorescence Microscopy Core Facility (NCCR Shared Equipment Grant No. 1S10RR024761-01). Ken Boucher of the Biostatistics Shared Resource at the Huntsman Cancer Institute provided guidance with statistical analysis. Haley Halberg and Ioana Pop provided valuable assistance with image processing and analysis. We appreciate reagents shared by Jon Dean at the University of Oxford, United Kingdom, and Matthias Gaestel at the Hannover Medical School, Germany. Diana Lim provided expert figure design and preparation. This work was supported by the National Institutes of Health (R01-GM50877 to M.C.B.) and the Huntsman Cancer Foundation. The Cancer Center Support Grant (2-P30-CA042014) awarded to the Huntsman Cancer Institute provided developmental funds and supported shared resources critical to this project.

REFERENCES

Aikawa R, Nagai T, Kudoh S, Zou Y, Tanaka M, Tamura M, Akazawa H, Takano H, Nagai R, Komuro I (2002). Integrins play a critical role in mechanical stress-induced p38 MAPK activation. Hypertension 39, 233–238.

An SS, Fabry B, Mellema M, Bursac P, Gerthoffer WT, Kayyali US, Gaestel M, Shore SA, Fredberg JJ (2004). Role of heat shock protein 27 in cytoskeletal remodeling of the airway smooth muscle cell. J Appl Physiol 96, 1701–1713.

Ateshian GA, Humphrey JD (2012). Continuum mixture models of biological growth and remodeling: past successes and future opportunities. Annu Rev Biomed Eng 14, 97–111.

Beckerle MC (1986). Identification of a new protein localized at sites of cell-substrate adhesion. J Cell Biol 103, 1679–1687.

Benndorf R, Hayess K, Ryazantsev S, Wieske M, Behlke J, Lutsch G (1994). Phosphorylation and supramolecular organization of murine small heat shock protein HSP25 abolish its actin polymerization-inhibiting activity. J Biol Chem 269, 20780–20784.

Boudreault F, Tschumperlin DJ (2010). Stretch-induced mitogen-activated protein kinase activation in lung fibroblasts is independent of receptor tyrosine kinases. Am J Respir Cell Mol Biol 43, 64–73.

Brown SS, Spudich JA (1981). Mechanism of action of cytochalasin: evidence that it binds to actin filament ends. J Cell Biol 88, 487–491.

Bryantsev AL, Loktionova SA, Ilyinskaya OP, Tararak EM, Kampinga HH, Kabakov AE (2002). Distribution, phosphorylation, and activities of Hsp25 in heat-stressed H9c2 myoblasts: a functional link to cytoprotection. Cell Stress Chaperones 7, 146–155.

Burridge K, Fath K, Kelly T, Nuckolls G, Turner C (1988). Focal adhesions: transmembrane junctions between the extracellular matrix and the cytoskeleton. Annu Rev Cell Biol 4, 487–525.

Byers HR, White GE, Fujiwara K (1984). Organization and function of stress fibers in cells in vitro and in situ. A review. Cell Muscle Motil 5, 83–137.

Chapin LM, Blankman E, Smith MA, Shiu YT, Beckerle MC (2012). Lateral communication between stress fiber sarcomeres facilitates a local remodeling response. Biophys J 103, 2082–2092.

Chaudhuri S, Smith PG (2008). Cyclic strain-induced HSP27 phosphorylation modulates actin filaments in airway smooth muscle cells. Am J Respir Cell Mol Biol 39, 270–278.

Chen CS (2008). Mechanotransduction - a field pulling together? J Cell Sci 121, 3285–3292.

Clarke JP, Mearow KM (2013). Cell stress promotes the association of phosphorylated HspB1 with F-actin. PLoS One 8, e68978.

Cohen TS, Gray Lawrence G, Khasgiwala A, Margulies SS (2010). MAPK activation modulates permeability of isolated rat alveolar epithelial cell monolayers following cyclic stretch. PLoS One 5, e10385.

Collier NC, Schlesinger MJ (1986). The dynamic state of heat shock proteins in chicken embryo fibroblasts. J Cell Biol 103, 1495–1507.

Colombelli J, Besser A, Kress H, Reynaud EG, Girard P, Caussinus E, Haselmann U, Small JV, Schwarz US, Stelzer EH (2009). Mechanosensing in actin stress fibers revealed by a close correlation between force and protein localization. J Cell Sci 122, 1665–1679.

Cooper JA (1987). Effects of cytochalasin and phalloidin on actin. J Cell Biol 105, 1473–1478.

Crawford AW, Beckerle MC (1991). Purification and characterization of zyxin, an 82,000-dalton component of adherens junctions. J Biol Chem 266, 5847–5853.

Crowe J, Aubareda A, McNamee K, Przybycien PM, Lu X, Williams RO, Bou-Gharios G, Saklatvala J, Dean JL (2013). Heat shock protein B1-deficient mice display impaired wound healing. PLoS One 8, e77383.

Cuadrado A, Nebreda AR (2010). Mechanisms and functions of p38 MAPK signalling. Biochem J 429, 403–417.

Cuenda A, Rouse J, Doza YN, Meier R, Cohen P, Gallagher TF, Young PR, Lee JC (1995). SB 203580 is a specific inhibitor of a MAP kinase homologue which is stimulated by cellular stresses and interleukin-1. FEBS Letters 364, 229–233.

Damarla M, Hasan E, Boueiz A, Le A, Pae HH, Montouchet C, Kolb T, Simms T, Myers A, Kayyali US, *et al.* (2009). Mitogen activated protein kinase activated protein kinase 2 regulates actin polymerization and vascular leak in ventilator associated lung injury. PLoS One 4, e4600.

Deanfield JE, Halcox JP, Rabelink TJ (2007). Endothelial function and dysfunction: testing and clinical relevance. Circulation 115, 1285–1295.

del Rio A, Perez-Jimenez R, Liu R, Roca-Cusachs P, Fernandez JM, Sheetz MP (2009). Stretching single talin rod molecules activates vinculin binding. Science 323, 638–641.

Dent EW, Gertler FB (2003). Cytoskeletal dynamics and transport in growth cone motility and axon guidance. Neuron 40, 209–227.

Discher DE, Mooney DJ, Zandstra PW (2009). Growth factors, matrices, and forces combine and control stem cells. Science 324, 1673–1677.

Dolinay T, Wu W, Kaminski N, Ifedigbo E, Kaynar AM, Szilasi M, Watkins SC, Ryter SW, Hoetzel A, Choi AM (2008). Mitogen-activated protein kinases regulate susceptibility to ventilator-induced lung injury. PLoS One 3, e1601.

During RL, Gibson BG, Li W, Bishai EA, Sidhu GS, Landry J, Southwick FS (2007). Anthrax lethal toxin paralyzes actin-based motility by blocking Hsp27 phosphorylation. EMBO J 26, 2240–2250.

Ehrlicher AJ, Nakamura F, Hartwig JH, Weitz DA, Stossel TP (2011). Mechanical strain in actin networks regulates FilGAP and integrin binding to filamin A. Nature 478, 260–263.

Ellis RJ, Hemmingsen SM (1989). Molecular chaperones: proteins essential for the biogenesis of some macromolecular structures. Trends Biochem Sci 14, 339–342.

Evgrafov OV, Mersiyanova I, Irobi J, Van Den Bosch L, Dierick I, Leung CL, Schagina O, Verpoorten N, Van Impe K, Fedotov V, *et al.* (2004). Mutant small heat-shock protein 27 causes axonal Charcot-Marie-Tooth disease and distal hereditary motor neuropathy. Nat Genet 36, 602–606.

Flanagan MD, Lin S (1980). Cytochalasins block actin filament elongation by binding to high affinity sites associated with F-actin. J Biol Chem 255, 835–838.

Fournier MF, Sauser R, Ambrosi D, Meister JJ, Verkhovsky AB (2010). Force transmission in migrating cells. J Cell Biol 188, 287–297.

Galkin VE, Orlova A, Egelman EH (2012). Actin filaments as tension sensors. Curr Biol 22, R96–R101.

Geiger B, Spatz JP, Bershadsky AD (2009). Environmental sensing through focal adhesions. Nat Rev Mol Cell Biol 10, 21–33.

Gerthoffer WT, Gunst SJ (2001). Invited review: focal adhesion and small heat shock proteins in the regulation of actin remodeling and contractility in smooth muscle. J Appl Physiol 91, 963–972.

Guay J, Lambert H, Gingras-Breton G, Lavoie JN, Huot J, Landry J (1997). Regulation of actin filament dynamics by p38 map kinase-mediated phosphorylation of heat shock protein 27. J Cell Sci 110(Pt 3), 357–368.

Guo WH, Wang YL (2007). Retrograde fluxes of focal adhesion proteins in response to cell migration and mechanical signals. Mol Biol Cell 18, 4519–4527.

Gupton SL, Eisenmann K, Alberts AS, Waterman-Storer CM (2007). mDia2 regulates actin and focal adhesion dynamics and organization in the lamella for efficient epithelial cell migration. J Cell Sci 120, 3475–3487.

Harris AK, Wild P, Stopak D (1980). Silicone rubber substrata: a new wrinkle in the study of cell locomotion. Science 208, 177–179.

Hayakawa K, Tatsumi H, Sokabe M (2011). Actin filaments function as a tension sensor by tension-dependent binding of cofilin to the filament. J Cell Biol 195, 721–727.

Hirata H, Tatsumi H, Sokabe M (2008). Mechanical forces facilitate actin polymerization at focal adhesions in a zyxin-dependent manner. J Cell Sci 121, 2795–2804.

Hoffman LM, Jensen CC, Chaturvedi A, Yoshigi M, Beckerle MC (2012). Stretch-induced actin remodeling requires targeting of zyxin to stress fibers and recruitment of actin regulators. Mol Biol Cell 23, 1846–1859.

Hoffman LM, Jensen CC, Kloeker S, Wang CL, Yoshigi M, Beckerle MC (2006). Genetic ablation of zyxin causes Mena/VASP mislocalization, increased motility, and deficits in actin remodeling. J Cell Biol 172, 771–782.

Hoffman LM, Nix DA, Benson B, Boot-Hanford R, Gustafsson E, Jamora C, Menzies AS, Goh KL, Jensen CC, Gertler FB, *et al.* (2003). Targeted disruption of the murine *zyxin* gene. Mol Cell Biol 23, 70–79.

Horton ER, Astudillo P, Humphries MJ, Humphries JD (2016). Mechanosensitivity of integrin adhesion complexes: role of the consensus adhesome. Exp Cell Res 343, 7–13.

Hotamisligil GS, Davis RJ (2016). Cell signaling and stress responses. Cold Spring Harb Perspect Biol 8.

Houlden H, Laura M, Wavrant-De Vrieze F, Blake J, Wood N, Reilly MM (2008). Mutations in the HSP27 (HSPB1) gene cause dominant, recessive, and sporadic distal HMN/CMT type 2. Neurology 71, 1660–1668.

Huot J, Houle F, Marceau F, Landry J (1997). Oxidative stress-induced actin reorganization mediated by the p38 mitogen-activated protein kinase/heat shock protein 27 pathway in vascular endothelial cells. Circ Res 80, 383–392.

Iskratsch T, Wolfenson H, Sheetz MP (2014). Appreciating force and shape-the rise of mechanotransduction in cell biology. Nat Rev Mol Cell Biol 15, 825–833.

Jakob U, Gaestel M, Engel K, Buchner J (1993). Small heat shock proteins are molecular chaperones. J Biol Chem 268, 1517–1520.
Kayyali US, Pennella CM, Trujillo C, Villa O, Gaestel M, Hassoun PM (2002). Cytoskeletal changes in hypoxic pulmonary endothelial cells are dependent on MAPK-activated protein kinase MK2. J Biol Chem 277, 42596–42602.
Kim-Kaneyama JR, Suzuki W, Ichikawa K, Ohki T, Kohno Y, Sata M, Nose K, Shibanuma M (2005). Uni-axial stretching regulates intracellular localization of Hic-5 expressed in smooth-muscle cells in vivo. J Cell Sci 118, 937–949.
Kuo JC, Han X, Hsiao CT, Yates JR 3rd, Waterman CM (2011). Analysis of the myosin-II-responsive focal adhesion proteome reveals a role for beta-Pix in negative regulation of focal adhesion maturation. Nat Cell Biol 13, 383–393.
Landry J, Huot J (1995). Modulation of actin dynamics during stress and physiological stimulation by a signaling pathway involving p38 MAP kinase and heat-shock protein 27. Biochem Cell Biol 73, 703–707.
Lauffenburger DA, Horwitz AF (1996). Cell migration: a physically integrated molecular process. Cell 84, 359–369.
Lavoie JN, Lambert H, Hickey E, Weber LA, Landry J (1995). Modulation of cellular thermoresistance and actin filament stability accompanies phosphorylation-induced changes in the oligomeric structure of heat shock protein 27. Mol Cell Biol 15, 505–516.
Li S, Piotrowicz RS, Levin EG, Shyy YJ, Chien S (1996). Fluid shear stress induces the phosphorylation of small heat shock proteins in vascular endothelial cells. Am J Physiol 271, C994–C1000.
Luxton GW, Gomes ER, Folker ES, Worman HJ, Gundersen GG (2011). TAN lines: a novel nuclear envelope structure involved in nuclear positioning. Nucleus 2, 173–181.
Mammoto A, Mammoto T, Ingber DE (2012). Mechanosensitive mechanisms in transcriptional regulation. J Cell Sci 125, 3061–3073.
McGough A, Pope B, Chiu W, Weeds A (1997). Cofilin changes the twist of F-actin: implications for actin filament dynamics and cellular function. J Cell Biol 138, 771–781.
Miron T, Vancompernolle K, Vandekerckhove J, Wilchek M, Geiger B (1991). A 25-kD inhibitor of actin polymerization is a low molecular mass heat shock protein. J Cell Biol 114, 255–261.
Miron T, Wilchek M, Geiger B (1988). Characterization of an inhibitor of actin polymerization in vinculin-rich fraction of turkey gizzard smooth muscle. Eur J Biochem 178, 543–553.
Mounier N, Arrigo AP (2002). Actin cytoskeleton and small heat shock proteins: how do they interact? Cell Stress Chaperones 7, 167–176.
Mymrikov EV, Seit-Nebi AS, Gusev NB (2011). Large potentials of small heat shock proteins. Physiol Rev 91, 1123–1159.
Nguyen HT, Adam RM, Bride SH, Park JM, Peters CA, Freeman MR (2000). Cyclic stretch activates p38 SAPK2-, ErbB2-, and AT1-dependent signaling in bladder smooth muscle cells. Am J Physiol Cell Physiol 279, C1155–C1167.
Parker KK, Brock AL, Brangwynne C, Mannix RJ, Wang N, Ostuni E, Geisse NA, Adams JC, Whitesides GM, Ingber DE (2002). Directional control of lamellipodia extension by constraining cell shape and orienting cell tractional forces. FASEB J 16, 1195–1204.
Peng GE, Wilson SR, Weiner OD (2011). A pharmacological cocktail for arresting actin dynamics in living cells. Mol Biol Cell 22, 3986–3994.
Ran FA, Hsu PD, Wright J, Agarwala V, Scott DA, Zhang F (2013). Genome engineering using the CRISPR-Cas9 system. Nat Protoc 8, 2281–2308.
Rape AD, Guo WH, Wang YL (2011). The regulation of traction force in relation to cell shape and focal adhesions. Biomaterials 32, 2043–2051.
Richard MN, Deniset JF, Kneesh AL, Blackwood D, Pierce GN (2007). Mechanical stretching stimulates smooth muscle cell growth, nuclear protein import, and nuclear pore expression through mitogen-activated protein kinase activation. J Biol Chem 282, 23081–23088.
Rodriguez-Carballo E, Gamez B, Ventura F (2016). p38 MAPK signaling in osteoblast differentiation. Front Cell Dev Biol 4, 40.
Ronkina N, Kotlyarov A, Dittrich-Breiholz O, Kracht M, Hitti E, Milarski K, Askew R, Marusic S, Lin LL, Gaestel M, Telliez JB (2007). The mitogen-activated protein kinase (MAPK)-activated protein kinases MK2 and MK3 cooperate in stimulation of tumor necrosis factor biosynthesis and stabilization of p38 MAPK. Mol Cell Biol 27, 170–181.
Rothman JE (1989). Polypeptide chain binding proteins: catalysts of protein folding and related processes in cells. Cell 59, 591–601.
Salinthone S, Tyagi M, Gerthoffer WT (2008). Small heat shock proteins in smooth muscle. Pharmacol Ther 119, 44–54.
Sawada Y, Nakamura K, Doi K, Takeda K, Tobiume K, Saitoh M, Morita K, Komuro I, De Vos K, Sheetz M, Ichijo H (2001). Rap1 is involved in cell stretching modulation of p38 but not ERK or JNK MAP kinase. J Cell Sci 114, 1221–1227.
Sawada Y, Tamada M, Dubin-Thaler BJ, Cherniavskaya O, Sakai R, Tanaka S, Sheetz MP (2006). Force sensing by mechanical extension of the Src family kinase substrate p130Cas. Cell 127, 1015–1026.
Schiller HB, Friedel CC, Boulegue C, Fassler R (2011). Quantitative proteomics of the integrin adhesome show a myosin II-dependent recruitment of LIM domain proteins. EMBO Rep 12, 259–266.
Shimozawa T, Ishiwata S (2009). Mechanical distortion of single actin filaments induced by external force: detection by fluorescence imaging. Biophys J 96, 1036–1044.
Smith MA, Blankman E, Deakin NO, Hoffman LM, Jensen CC, Turner CE, Beckerle MC (2013). LIM domains target actin regulators paxillin and zyxin to sites of stress fiber strain. PLoS One 8, e69378.
Smith MA, Blankman E, Gardel ML, Luettjohann L, Waterman CM, Beckerle MC (2010). A zyxin-mediated mechanism for actin stress fiber maintenance and repair. Dev Cell 19, 365–376.
Smith MA, Hoffman LM, Beckerle MC (2014). LIM proteins in actin cytoskeleton mechanoresponse. Trends Cell Biol 24, 575–583.
Sousa AM, Liu T, Guevara O, Stevens J, Fanburg BL, Gaestel M, Toksoz D, Kayyali US (2007). Smooth muscle alpha-actin expression and myofibroblast differentiation by TGFbeta are dependent upon MK2. J Cell Biochem 100, 1581–1592.
Stokoe D, Engel K, Campbell DG, Cohen P, Gaestel M (1992). Identification of MAPKAP kinase 2 as a major enzyme responsible for the phosphorylation of the small mammalian heat shock proteins. FEBS Lett 313, 307–313.
Symons MH, Mitchison TJ (1991). Control of actin polymerization in live and permeabilized fibroblasts. J Cell Biol 114, 503–513.
Uyeda TQ, Iwadate Y, Umeki N, Nagasaki A, Yumura S (2011). Stretching actin filaments within cells enhances their affinity for the myosin II motor domain. PLoS One 6, e26200.
Wang J, Fan J, Laschinger C, Arora PD, Kapus A, Seth A, McCulloch CA (2005). Smooth muscle actin determines mechanical force-induced p38 activation. J Biol Chem 280, 7273–7284.
Wang N, Butler JP, Ingber DE (1993). Mechanotransduction across the cell surface and through the cytoskeleton. Science 260, 1124–1127.
Wang N, Ostuni E, Whitesides GM, Ingber DE (2002). Micropatterning tractional forces in living cells. Cell Motil Cytoskeleton 52, 97–106.
Wong AJ, Pollard TD, Herman IM (1983). Actin filament stress fibers in vascular endothelial cells in vivo. Science 219, 867–869.
Wozniak MA, Chen CS (2009). Mechanotransduction in development: a growing role for contractility. Nat Rev Mol Cell Biol 10, 34–43.
Yan J, Yao M, Goult BT, Sheetz MP (2015). Talin dependent mechanosensitivity of cell focal adhesions. Cell Mol Bioeng 8, 151–159.
Yoshigi M, Clark EB, Yost HJ (2003). Quantification of stretch-induced cytoskeletal remodeling in vascular endothelial cells by image processing. Cytometry A 55, 109–118.
Yoshigi M, Hoffman LM, Jensen CC, Yost HJ, Beckerle MC (2005). Mechanical force mobilizes zyxin from focal adhesions to actin filaments and regulates cytoskeletal reinforcement. J Cell Biol 171, 209–215.
Young PR, McLaughlin MM, Kumar S, Kassis S, Doyle ML, McNulty D, Gallagher TF, Fisher S, McDonnell PC, Carr SA, *et al*. (1997). Pyridinyl imidazole inhibitors of p38 mitogen-activated protein kinase bind in the ATP site. J Biol Chem 272, 12116–12121.
Zhang D, Gaussin V, Taffet GE, Belaguli NS, Yamada M, Schwartz RJ, Michael LH, Overbeek PA, Schneider MD (2000). TAK1 is activated in the myocardium after pressure overload and is sufficient to provoke heart failure in transgenic mice. Nat Med 6, 556–563.